GEORGIA INSTITUTE OF TECHNOLOGY
OFFICE OF CONTRACT ADMINISTRATION
SPONSORED PROJECT INITIATION

Date: 8/21/79

Project Title: Evaluation & Characterization Studies

Project No: A-2415

Project Director: Dr. Billy R. Livesay

Sponsor: Department of the Navy - Naval Weapons Center

Agreement Period: From 7/12/79 Until 9/30/79

Type Agreement: Purchase Order #N60530-79-M-DP46

Amount: $3,000

Reports Required: Measurements

Sponsor Contact Person (s):

Technical Matters

Mr. H. F. Blazek
Naval Weapons Center
China Lake, CA 93555

Contractual Matters
(thru OCA)

Administrative
Ms. Muriel Dodge
Contracting Officer
Naval Weapons Center
China Lake, CA 93555

Defense Priority Rating:

Assigned to: EML/SSSD (School/Laboratory)

COPIES TO:

- Project Director
- Division Chief (EES)
- School/Laboratory Director
- Dean/Director—EES
- Accounting Office
- Procurement Office
- Security Coordinator (OCA)
- Reports Coordinator (OCA)
- Library, Technical Reports Section
- EES Information Office
- EES Reports & Procedures
- Project File (OCA)
- Project Code (GTRI)
- Other

CA-3 (3/76)

GEORGIA INSTITUTE OF TECHNOLOGY OFFICE OF CONTRACT ADMINISTRATION

SPONSORED PROJECT TERMINATION SHEET

Date 11/1/82

Project Title: Evaluation & Characterization Studies

Project No: A-2415

Project Director: Dr. Billy R. Livesay

Sponsor: Navy-Naval Weapons Center

Effective Termination Date: 9/30/79

Clearance of Accounting Charges: _____

Grant/Contract Closeout Actions Remaining:

- [x] Final Invoice and Closing Documents
- [ ] Final Fiscal Report
- [x] Final Report of Inventions
- [x] Govt. Property Inventory & Related Certificate
- [ ] Classified Material Certificate
- [ ] Other _____

NOTE: Final Report delivered directly to sponsor in August 1982.

Assigned to: EML (~~School~~/Laboratory)

COPIES TO:

Administrative Coordinator	Research Security Services	EES Public Relations (2)
Research Property Management	Reports Coordinator (OCA)	Computer Input
Accounting	Legal Services (OCA)	Project File
Procurement/EES Supply Services	Library	Other _____

FORM OCA 10:781

FRICTION AND WEAR IN COATED SPECIMENS

By
B. R. Livesay
Engineering Experiment Station
Physical Sciences Division
Georgia Institute of Technology

Project Conducted For
Naval Weapons Center
China Lake, California 93555

August 1982

FRICTION AND WEAR IN COATED SUBSTRATES

INTRODUCTION

The friction and wear characteristics of six stainless steel bearing specimens prepared at the Naval Weapons Center at China Lake, Ca, were measured using the experimental facilities of the Micromechanics Laboratory at the Georgia Institue of Technology. The measurements included coefficients of friction, wear resistance and microhardness. The coatings are intended to provide improved wear resistance, decreased friction or both. One set of specimens involved two coatings which potentially might provide an added interface strengthening mechanism or, at least, a harder surface phase.

The coefficient of friction measurements were made at stylus load levels up to about 100 dyne such that no observable damage occurred to the specimen surfaces. Similar load levels were employed with the accelerated wear test specimens. In the case of the accelerated wear specimens, times were selected such that observable wear damage was initiated in the test specimens.

MECHANISMS OF SLIDING WEAR

Wear processes occur between any two solid surfaces which are pressed together and displaced tangentially relative to one another. Tangential, or frictional, forces result from the surface-surface interactions due to relative motion. The resulting tangential reaction stresses within the surface regions of the respective materials give rise to mechanical damage mechanisms leading to material wear. Although the fundamental mechanical damage mechanisms involved in wear are not really different from those which occur in other structural materials under stress, the special geometrical considerations involved with rubbing surfaces are very complex and have thus made friction and wear into what is essentially a separate discipline. The basic area of friction and wear, now called "tribology," has been treated in a number of texts and does not require general discussion here.

The actual area of contact between two solids is normally much less than the apparent contacting area. This is because surface variations are always present, either on a macroscopic or a microscopic scale, and thus cause the load to be supported by surface asperities as indicated schematically in Figure 1. The analysis of friction and wear phenomena is therefore carried out by considering the forces and material response to asperity interactions. Since the actual area supporting the load is generally much, much smaller than the apparent contacting area, the microscopic mechanical stresses at the load supporting asperities may be quite large. The asperities and the material just below will be deformed either elastically or plastically, depending on both the loading and the properties of the interacting materials. With relative tangential motion, shear stresses are introduced, leading to still more complex microscopic stress distributions within the surface regions of the materials.

Frictional forces arise from the combined effect of adhesion and "plowing" in material regions of real contact. Many factors influence the adhesion of two metal surfaces. Carefully cleaned surfaces rubbing in ultra-high vacuum often firmly weld together upon contact. Even in the atmosphere, deformation of the metal will rupture surface oxides and allow sufficient free metal contact to form strong bonds. This type of event occurs in both thermocompression (ball bonding) and ultrasonic bonding processes as used in the fabrication of microcircuits. The elevated temperatures involved in thermocompression bonding machines allows extensive deformation at relatively low compressive stress levels while a corresponding softening of face centered cubic metals occurs at high ultrasonic energy densities. The compressive stress levels in wear surfaces are generally much lower than those for intentional bonding processes but tangential motion tends to promote the shearing of asperties to, at least temporarily, expose free metal surfaces. Friction and wear phenomena are then further complicated by the involvement of materials represented by corrosion products and other impurities, such as a moisture layer, which normally have properties quite different from those of the base metals. In fact, there are many cases where a strong oxide is counted on to provide important wear

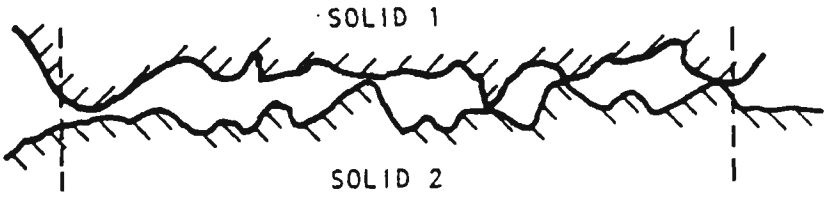

Figure 1. Schematic of Surface Asperities on Two Solids in Contact

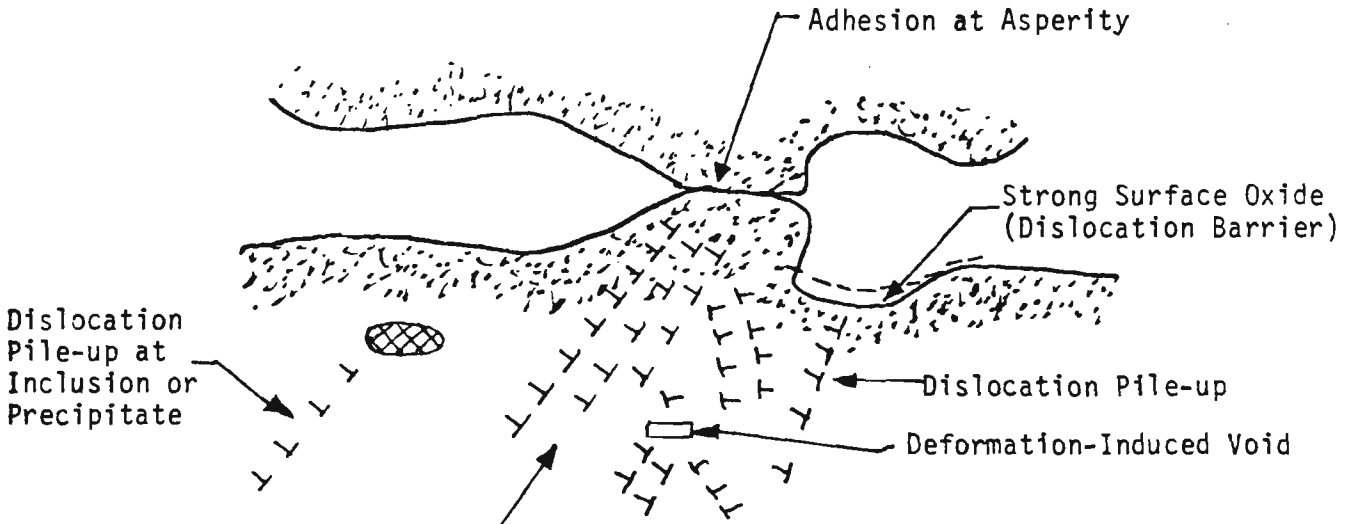

EARLY STATE OF PLASTIC DEFORMATION (BOTH SURFACES)

Figure 3. Stages in Wear Damage

protection for the surfaces of metal parts in service. Intentionally applied coatings or surface treatments are similarly recognized as offering great promise for being able to design special wear surfaces which greatly extend the life of a part relative to that of the base material. The technology developed during the last decade or two for applying desired coatings and implanting atomic species within a surface has greatly improved the prospects for developing highly wear resistant surfaces to fit many applications.

An additional factor which becomes important is that the composition and microstructural characteristics of the surface region of a metal or alloy may depart significantly from that of the bulk material. Surface segregation induced by a variety of physical and chemical driving forces is now recognized as a general occurrance and must be considered. Surface segregation will affect both the adhesive forces and the deformation modes which operate near the surface.

As indicated by the term, "plowing" involves the localized deformation of a softer material by asperities, or other features, on the harder surface. The plowing process is sometimes envisioned as a direct mechanical scraping of the softer surface. However, it is not likely that adhesion and plowing processes will ever occur independently where an fcc alloy is one of the metal wear pairs. The twelve available slip systems in face centered cubic metals generally include one or more systems oriented favorably for activation by an arbitrarily applied stress direction.

A cause-and-effect flowchart representing some of the likely stresses and material response factors involved in sliding wear is provided in Figure 2. The applied normal force causes compressive deformation at asperities and the tangential displacements introduce shear deformation. Of course, the slip within individual grains will take place along one or two critically oriented slip systems. The plastic deformation is illustrated schematically in Figure 3. Dislocation sources are activated by either the shear due to surface adhesion or the plowing term as well as by the applied normal force. The deformation of tiny asperities involves both elastic energy storage

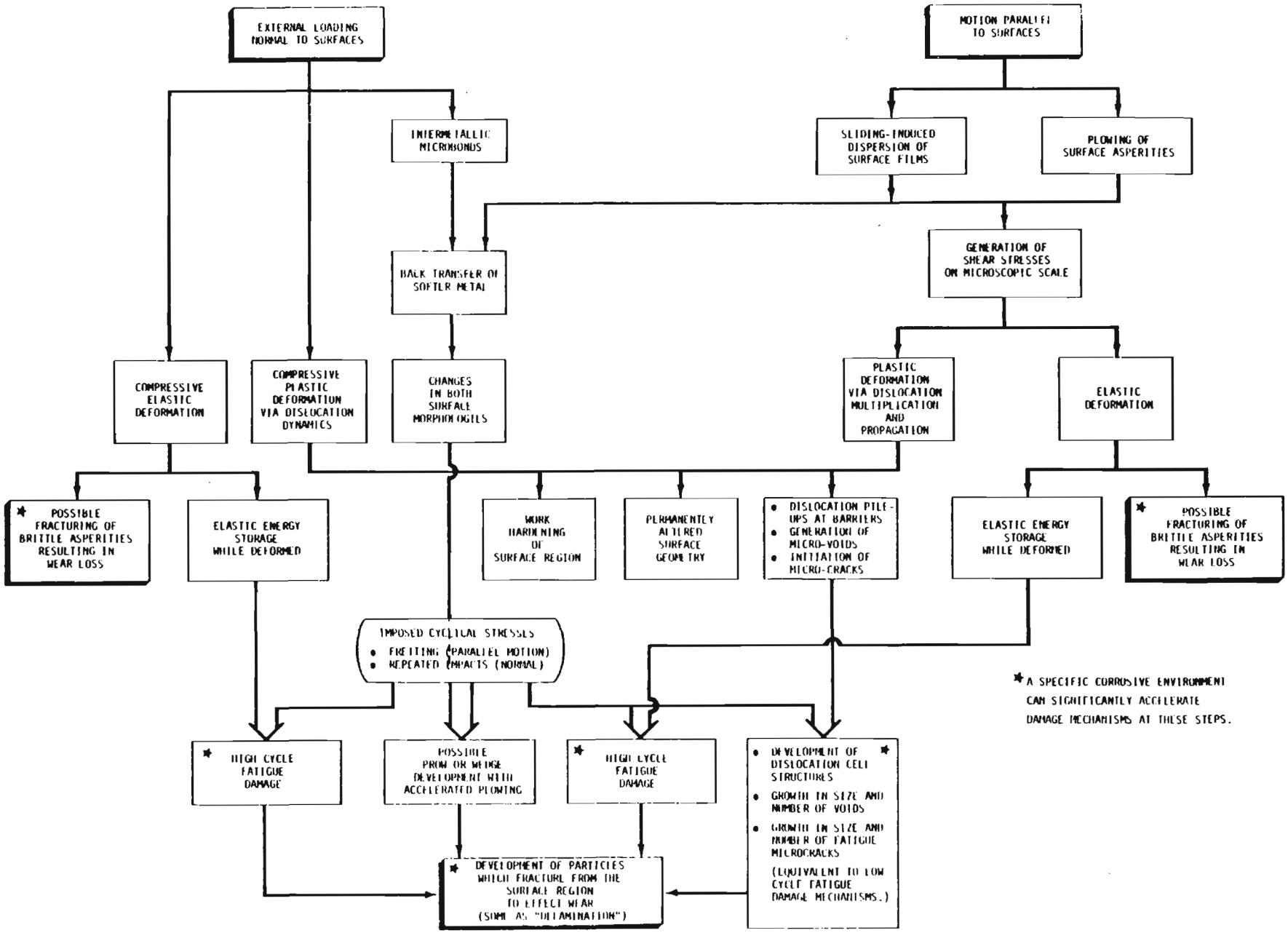

Figure 2. Mechanisms of Sliding Wear

and dislocation propagation. Subsequently, as the dislocation density becomes large, they begin to tangle, causing the surface region to work harden. The crystal structure has a striking effect on both friction and wear behavior as has been shown by studying cobalt on either side of its hcp-fcc crystal transition temperature. The wear rate of the fcc structure is about 100 times that of the same material with Co as hcp, which has only three slip systems. The schematic of Figure 3 also illustrates the effect of dislocation pile-up behind a suitable surface coating. The stress concentration at the lead dislocation often becomes sufficient to initiate microvoids which may grow into cracks. A more advanced state of the wear process is illustrated in Figure 4, where cracks or voids accumulate to cause the separation of particles from the surface.

The concept of a dense dislocation debris layer in the subsurface leading to voiding and cracks has been proposed and is reasonable. This then suggests a delamination type of wear which has been observed experimentally. Dense dislocation networks have been shown in micrographs in a plane parallel to the wear surface. There is often going to be a sufficiently strong and adherent oxide coating, as is the case for aluminum alloys, to repell dislocations unless the environment greatly alters the oxide properties. Applied coatings can provide strengthening of the resulting layered structure through several factors:

(a) Coating with greater elastic modulus than substrate.
(b) Different crystal structure.
(c) Solid solution in the interface.

These factors inhibit the transfer of dislocations through the interface and thereby increase the strength of the structure. However, it is essential that the coating form a coherent bond with the substrate for one of these strengthening mechanisms to be operable.

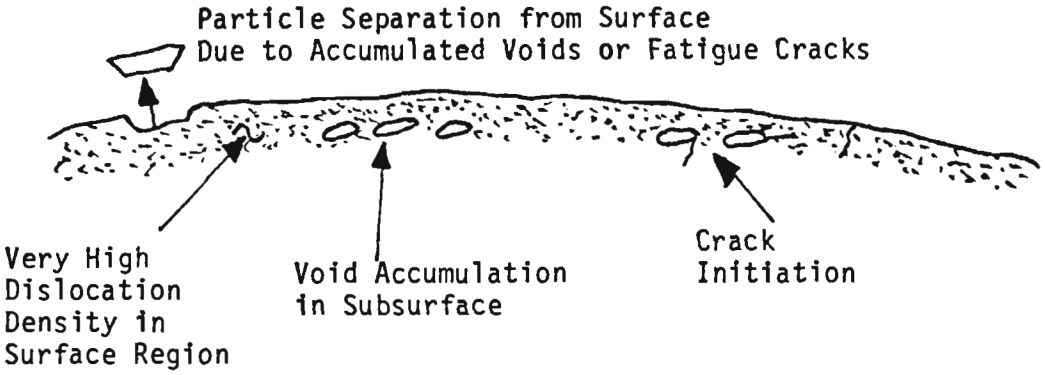

Figure 4. Advanced Stage of Plastic Deformation
(One Wear Surface)

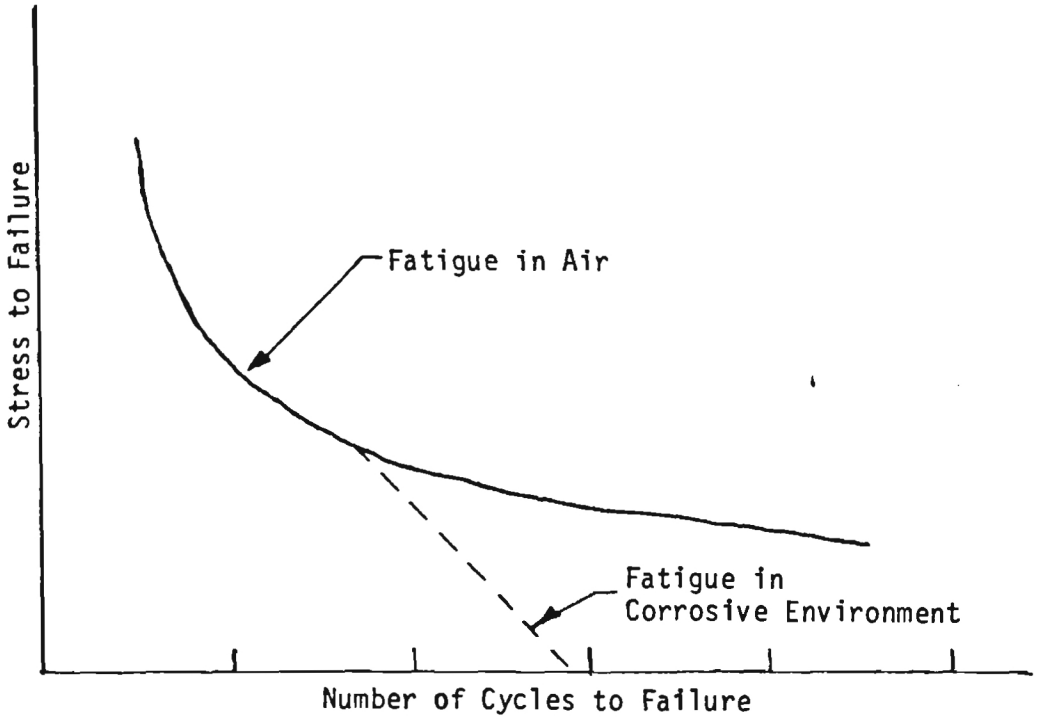

Figure 5. Typical S-N Fatigue Curve Showing Relative Effective
of Specific Environment on Fatigue Strength

Ion implantation bombards the surface and can greatly alter the arrangement of atoms within a few hundred atomic layers of the surface. For example, specific implanted ions can produce an alloy stoichiometry which is not normally achieved due to thermodynamic equilibrium and thereby greatly harden the surface region. Even bombardment with ions which do not take part in alloy strengthening processes can distort the crystalline arrangement of the surface region to cause hardening.

The formation of a "prow" or "wedge" on the surface of one wear member due to the back-transfer of material from the other member has been described by several investigators. While it is not found that all metal combinations will accumulate sufficient material by back-transfer for prow formation, it is a source of wear damage which must be examined for specific metal pairs in specific environments.

Most repetitive wear situations involve fatigue damage mechanisms. Fatigue failure mechanisms have been described extensively, and may usually be represented by an S-N curve similar to that shown in Figure 5. The effect of specific environments will drastically alter the shape of an S-N curve as indicated by the dotted lines in Figure 5. This phenomenon, called corrosion fatigue, is well established and often occurs unpredictably for particular alloy compositions or heat treatments when exposed to specific environmental conditons. Corrosion fatigue will significantly accelerate fatigue wear processes as indicated by the starred steps in Figure 2.

Attempts to derive an analytical expression to describe wear rates from fundamental mechanisms have not been very successful. The most widely accepted expression has been formulated by Archard which relates wear volume, V, sliding distance, X, normal load, L, and hardness, P. The Archard equation is:

$$V = K \frac{LX}{3P} \qquad (1)$$

Archard interprets the wear coefficient, K, in terms of the probability that a microweld at asperities will produce a wear fragment.

A similar equation has been advanced by Suh based on his delamination model of wear

$$V = kLX \tag{2}$$

where k is a wear factor given by

$$K = \frac{b}{4\pi}\left[\frac{K_1 G_1}{\sigma_{f_1} S_{o1}(1-\nu_1)} + \frac{K_2 G_2}{\sigma_{f_2} S_{o2}(1-\nu_2)}\right] \tag{3}$$

where
- b is the Burgers vector,
- ν_i is Poisson's ratio
- K_i is a constant depending upon surface topography,
- G_i is the shear modulus,
- σ_{fi} is the friction stress,
- S_{oi} is a critical sliding distance,

and the subscripts, 1 and 2, denote the two wear materials in contact.

A comparision of Equations 1 and 2 shows that k = K/3P. Both Archard's and Suh's equations thus relate the wear volume, V, to the mechanical energy dissipated, L.x, through a wear factor.

In some cases it is possible to experimentally determine the wear volume, V, by weight loss measurements. However, weight loss measurements are clearly not valid if the wear debris is not entirely removed from the wear surface, if there is an accumulation of corrosion products or if there is a back-transfer of material from the other wear member. Wear track profile analysis can be carried out using a precision profilometer, surface replica techniques or multiple sectioning of wear surfaces followed by optical or SEM measurements.

EXPERIMENTAL

The instrumentation of the Micromechanics Laboratory was employed to carry out three types of physical measurements on the six disc shaped specimens.

1. Friction
2. Accelerated Wear
3. Microhardness

The friction measurements were conducted using the low-load friction apparatus shown in Figure 6. This apparatus is capable of measuring frictional forces from less than 10^{-2} dyne to 10^{2} dyne. The normal force is applied electromagnetically by the D'Arsonval device seen in Figure 6 and the horizontal displacement is accomplished by a micrometer screw drive powered by synchronous motors. The frictional force is measured by an automatic balancing mechanism based on a galvanometer and an electro optical system. For these measurements, a stylus of 304SS wire was bent into the shape shown in Figure 7 and carefully polished. One of the wear specimen discs is shown supported by the normal force loading mechanism just above the SS stylus. During a friction run, any desired normal force is simply dialed into the instrument control package. The friction forces were monitored using an X-Y recorder.

The response of this system is sufficient to record details of the stick-slip behavior which is characteristic of frictional interactions between dry solids. Some of these curves are illustrated in the Appendix. In addition, the apparatus also integrates the widely varying frictional forces to provide an average force for desired segments of a path. We may thus interpret the peaks of the stick-slip behavior in terms of either microweld forces or else momentary mechanical interlocking (static friction) whereas the average frictional force values are representative of "kinetic" friction.

A number of friction measurements were made for each of the six specimens at normal force values between 10 dyne and 100 dyne. Some of these curves are included in the Appendix. At these load levels there was

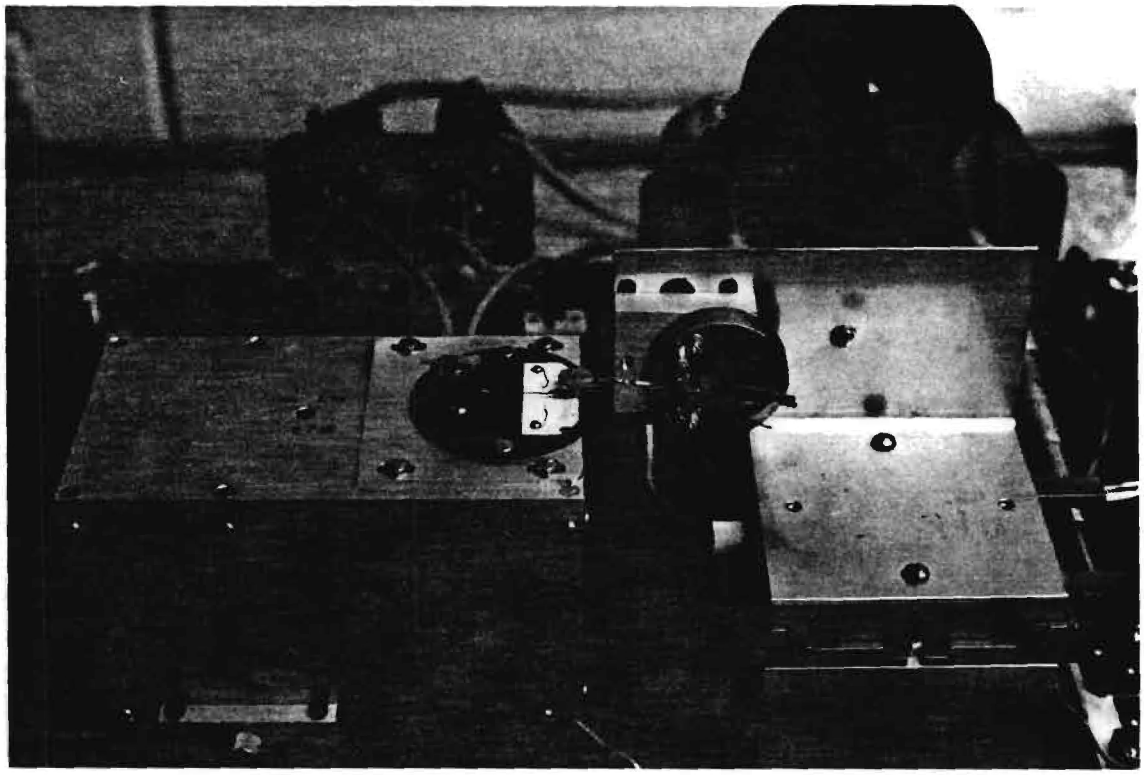

Figure 6. Low Load Friction Apparatus

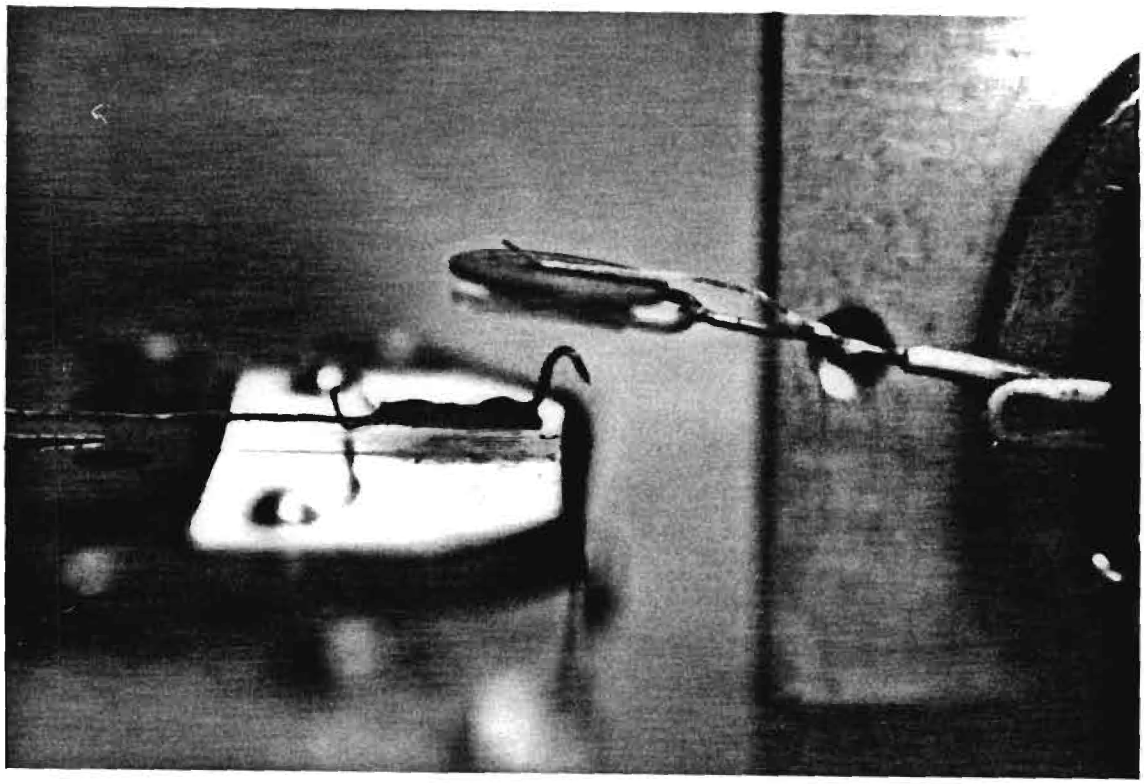

Figure 7. Planar Wear Specimen Above Wear Stylus

no detectable damage to the wear surfaces even though the various traces were carefully indexed and then examined both under the microscope and by a surface profilometer. Essentially, the surface roughness of the polished wear specimens was much greater than any damage caused by the small number of passes used for the friction force measurements. As a point of reference, single pass traces at these force levels are clearly seen in SEM micrographs for electropolished specimens of such soft metals as pure copper. For highly polished surfaces of soft metals we have been able to make direct correlations between details of the stick-slip friction curves and microscopic surface features and deformation. We were not able to do such direct correlation for the specimens studied here since the surface hardness apparently limited damage to levels very much smaller than the original surface roughness.

The kinetic friction coefficients for each of the six specimens are shown in Figures 8-13. These coefficients were computed from ratios of the average friction force and the applied normal load. In some cases the coefficients shown were averaged from several measurements at the same load.

The accelerated wear testing was carried out using the apparatus shown in Figure 14. The wear specimens were attached, as shown in Figure 15 to a vibrating arm driven by the electromagnetic transducer seen on the left side of the apparatus in Figure 14. A second wear member is pressed against the disc by an electromagnetic loading arrangement. Two stylus materials and two load levels were used with each specimen. One material was a sapphire phonographic stylus and the other a polished 304 stainless steel wire identical to that used for the friction measurements. The apparatus was set to vibrate at amplitudes of several mm with normal loads applied at 50 dyne and 25 dyne. The first wear track was with the sapphire stylus at a normal force of 50 dyne and was run with a total of 108,000 passes over the same path. After viewing wear scars, the subsequent tracks involved only 54,000 passes each. We were able to fit four wear tracks on each disc specimen and index their positions for later examantions using the profilometer, optical microscopy and SEM micrographs.

FIGURE 8

Friction Coefficient vs Load

SAMPLE 1 440-C BLANK

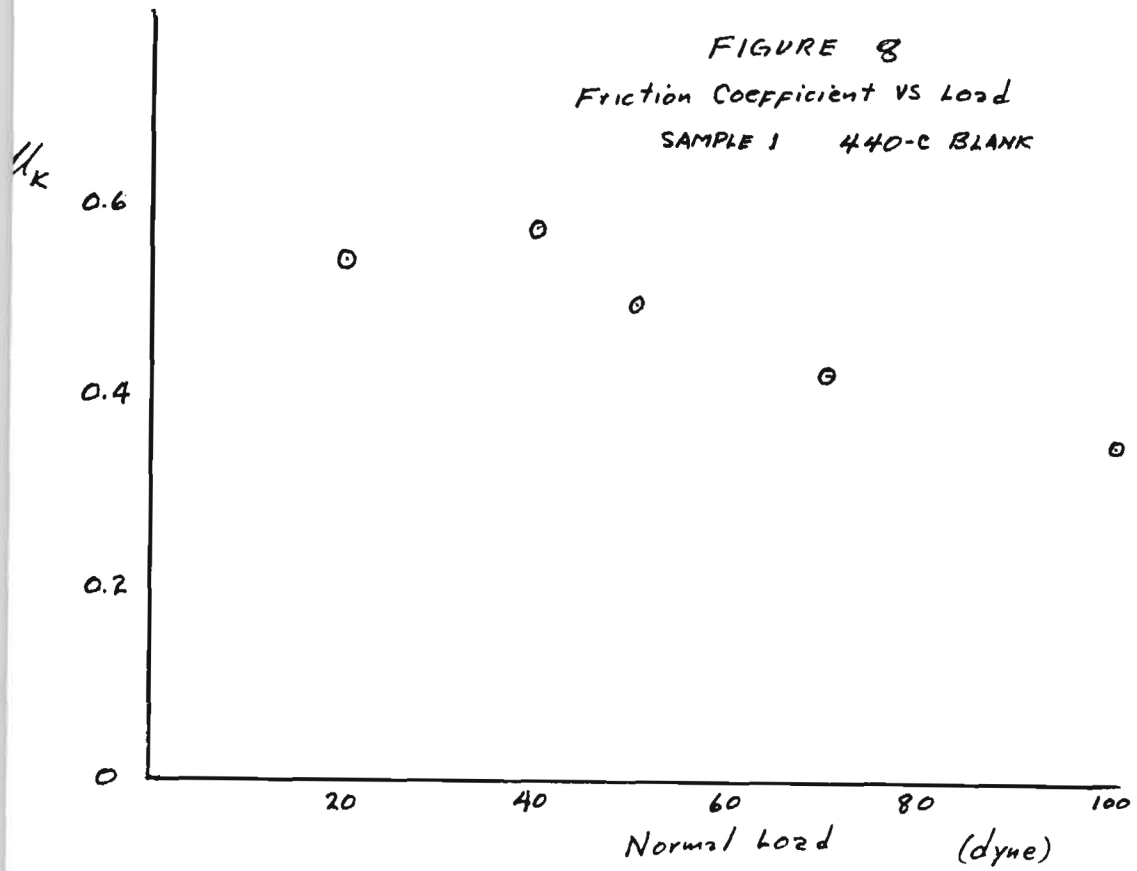

FIGURE 9

Friction Coefficient vs Load

SAMPLE 2 52100 SS BLANK

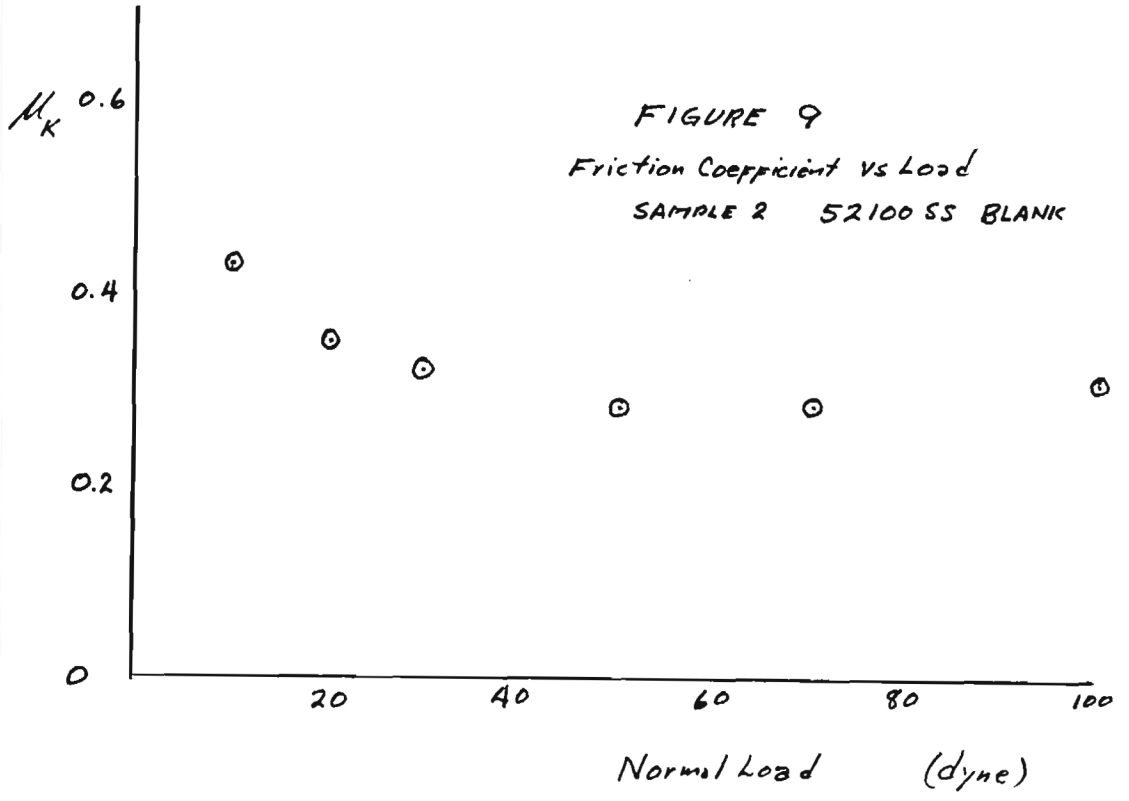

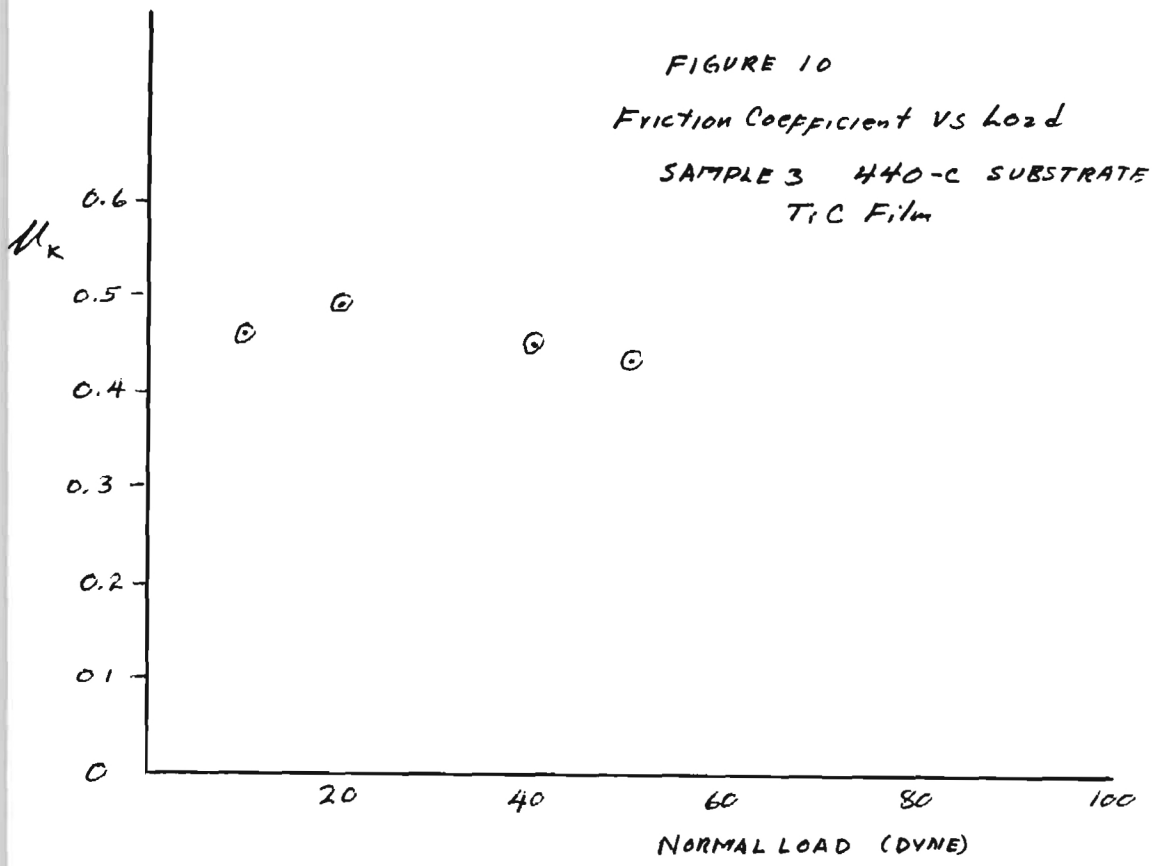

FIGURE 10

Friction Coefficient vs Load

SAMPLE 3 440-C SUBSTRATE
TiC Film

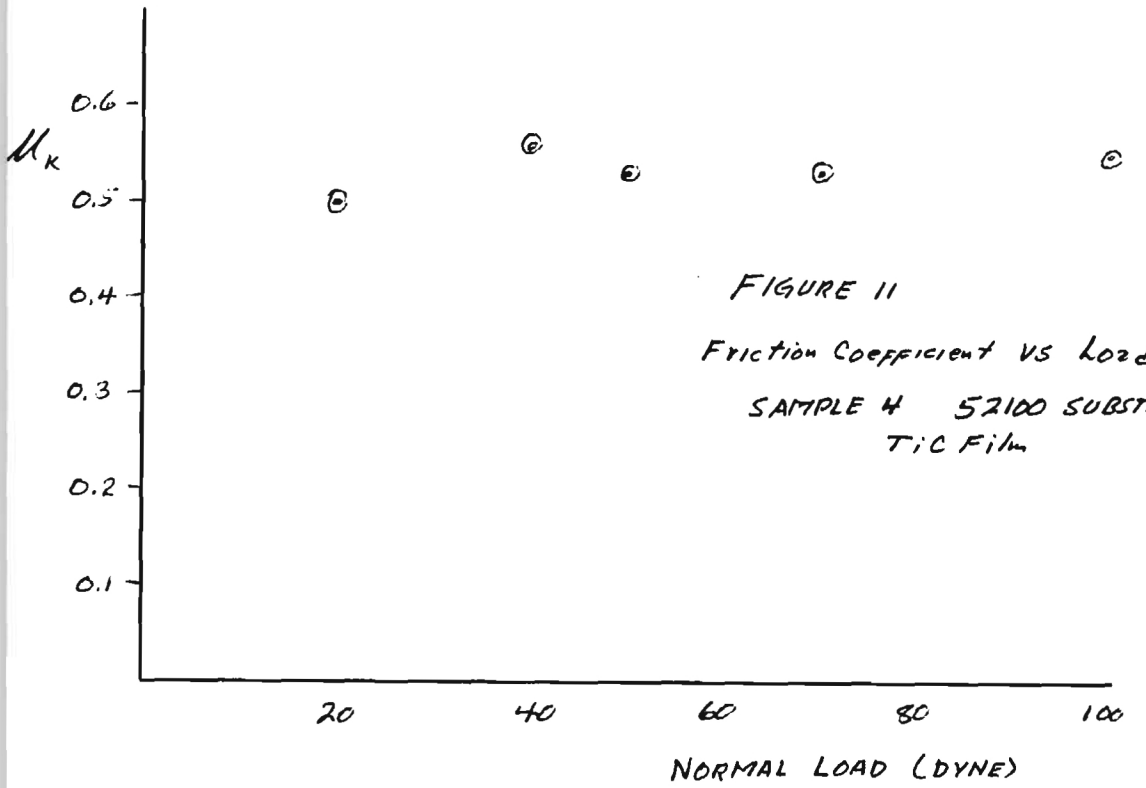

FIGURE 11

Friction Coefficient vs Load

SAMPLE 4 52100 SUBSTRATE
TiC Film

FIGURE 12

Friction Coefficient Vs Load

SAMPLE 5 440-C SUBSTRATE

TiC + TiNi Composite Film

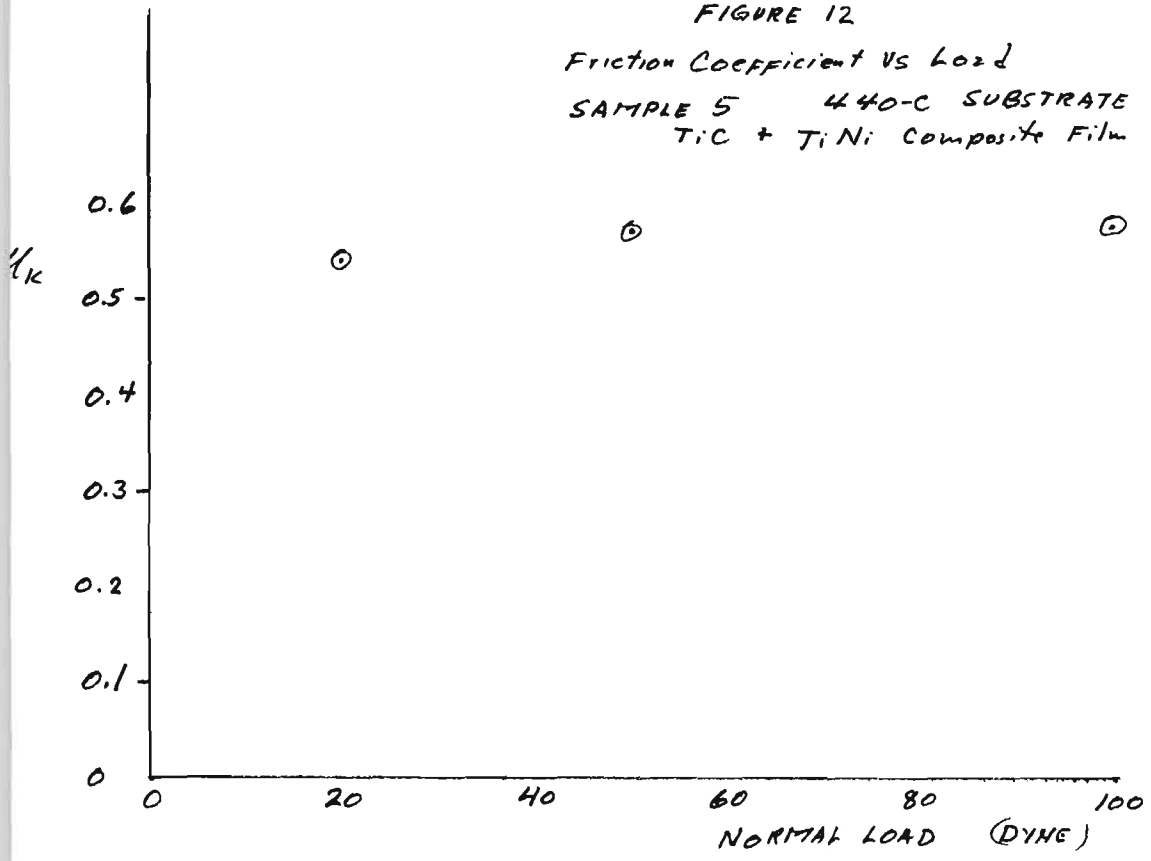

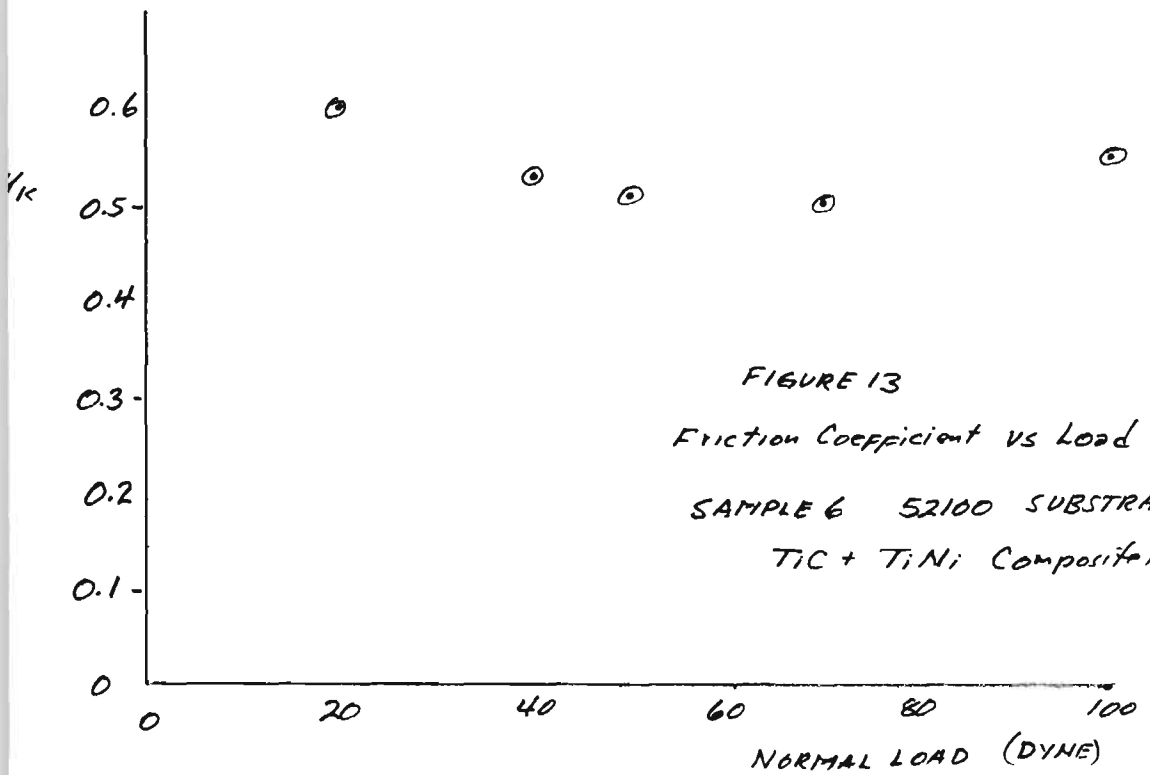

FIGURE 13

Friction Coefficient vs Load

SAMPLE 6 52100 SUBSTRATE

TiC + TiNi Composite Film

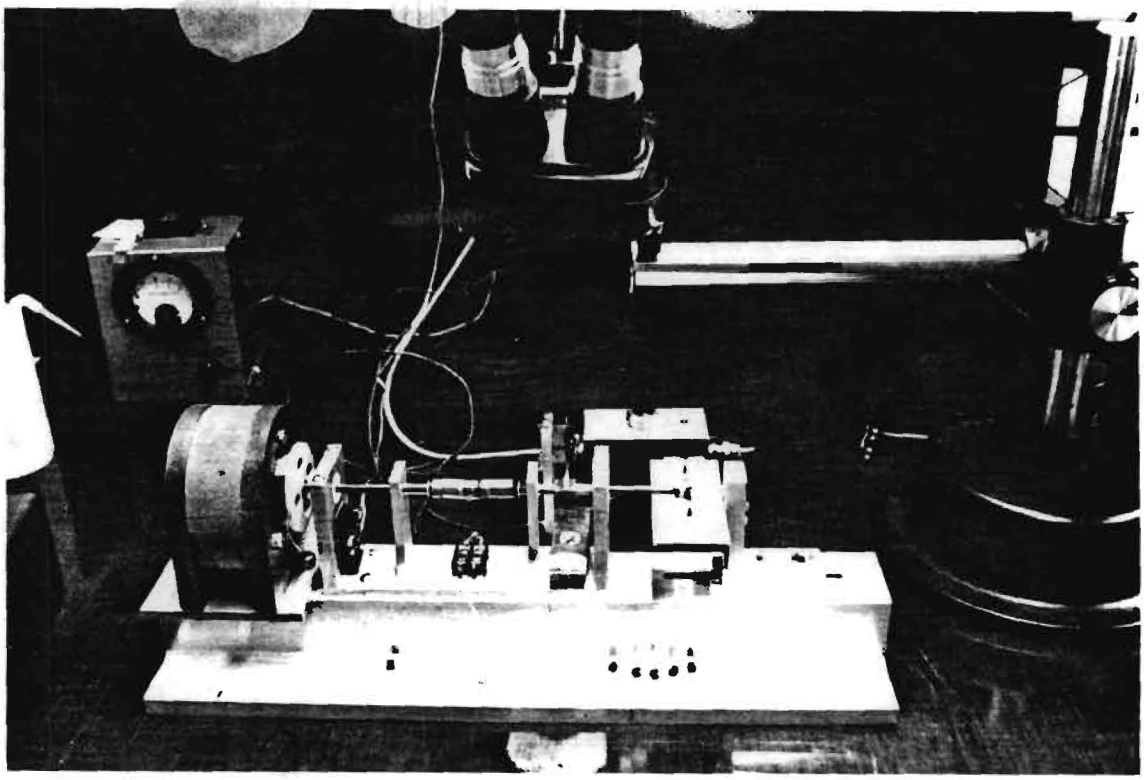

Figure 14. Accelerated Wear Test Apparatus

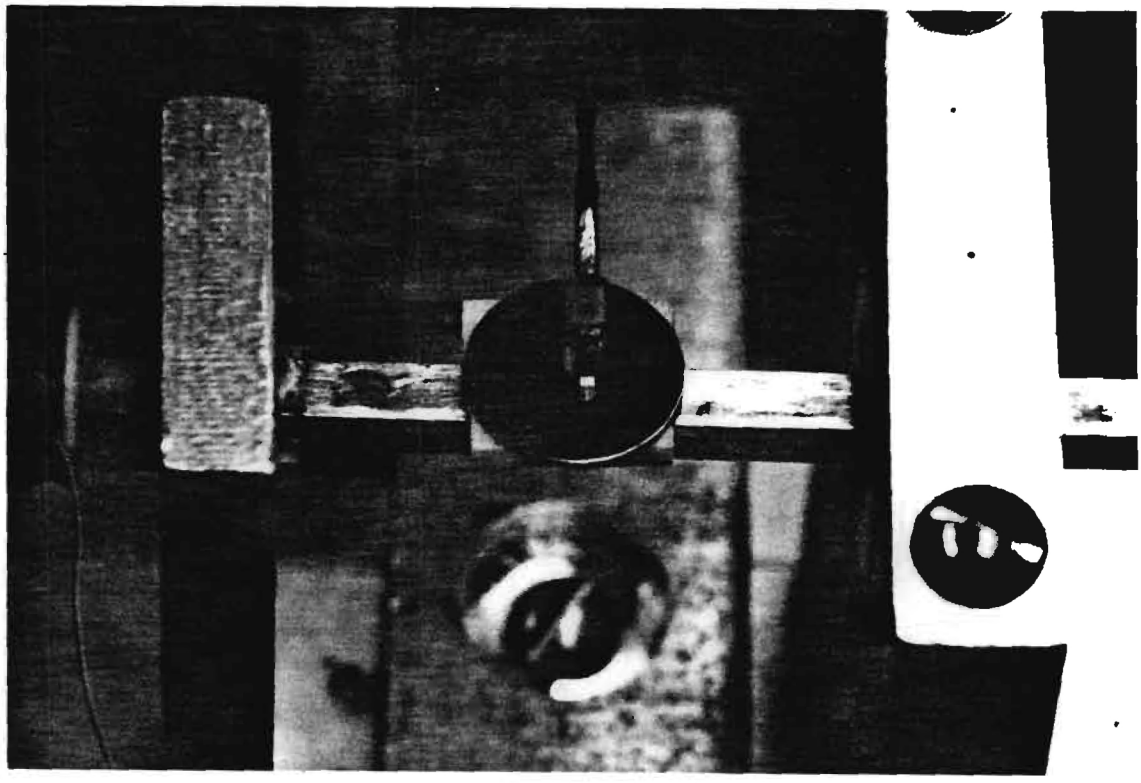

Figure 15. Accelerated Wear Test Specimen

The wear tracks were examined under optical microscopes, a scanning electron microscope and with a profilometer. The profilometer was manufactured by TENCOR Instruments with 1000Å full scale as its most sensitive range. The profilometer traces, which are included in the Appendix, were all made perpendicular to the particular wear track being examined. In most cases, a number of traces were made of each track in different sections of the track to obtain a more comprehensive quantitative view of the complete track. For example, the first sheet of profiles in the Appendix shows six different traces along the first track (sapphire stylus, 50 dyne, 108,000 passes). Two successive profile runs of the fourth trace are included on the sheet to illustrate the reproducibility of the profilometer data over precisely the same path. It is clear from these traces that details of the wear scars can vary significantly along a single wear track.

The identification symbols for each trace are defined in the Appendix. A depression on the surface is indicated by a downward deflection of the profile curve. In the horizontal direction the scale is 500 X. The profilometer traces clearly show that the wear damage to these surfaces is not a simple removal of material but rather involves a complex redistribution of material. It thus makes no sense to try fitting Archard's wear expression to these data.

SEM micrographs of some wear tracks are shown in Figures 16-28. The most severe wear is seen on the uncoated specimen (sample 2). Tracks 1 and 2 were abraded with the sapphire stylus. It appears that the material on this uncoated specimen is redistributed over the surface of the wear track. It is also clearly seen that a profilometer trace made at one point along a wear track will be different from that, in detail, at any other point. Wear in the coated specimens apparently initiates at weak points in the surface and grows from there.

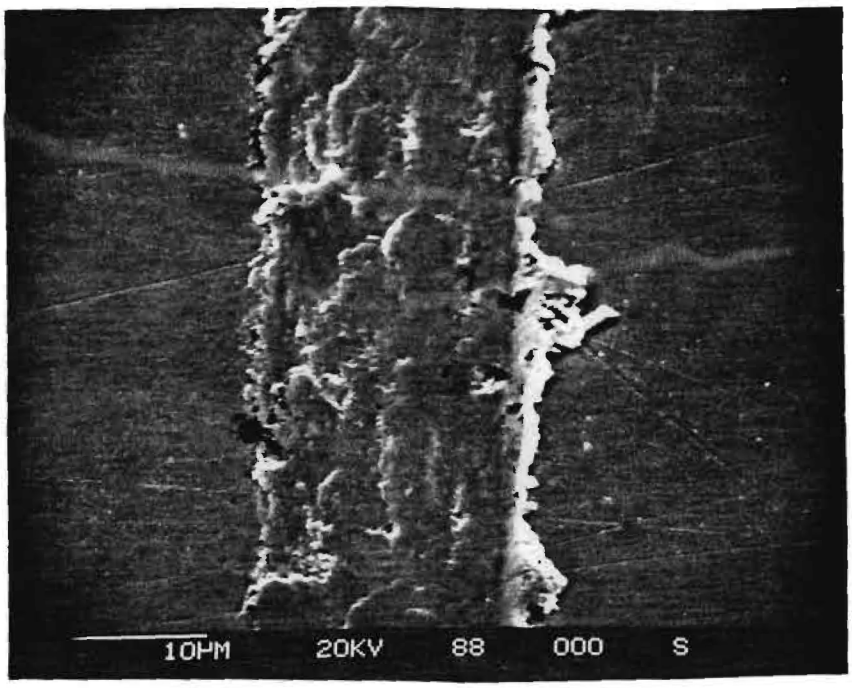

Figure 16. SEM Micrograph of Wear Scar. X2000 Sample 2, Track 1 (See Table 1 for Notation)

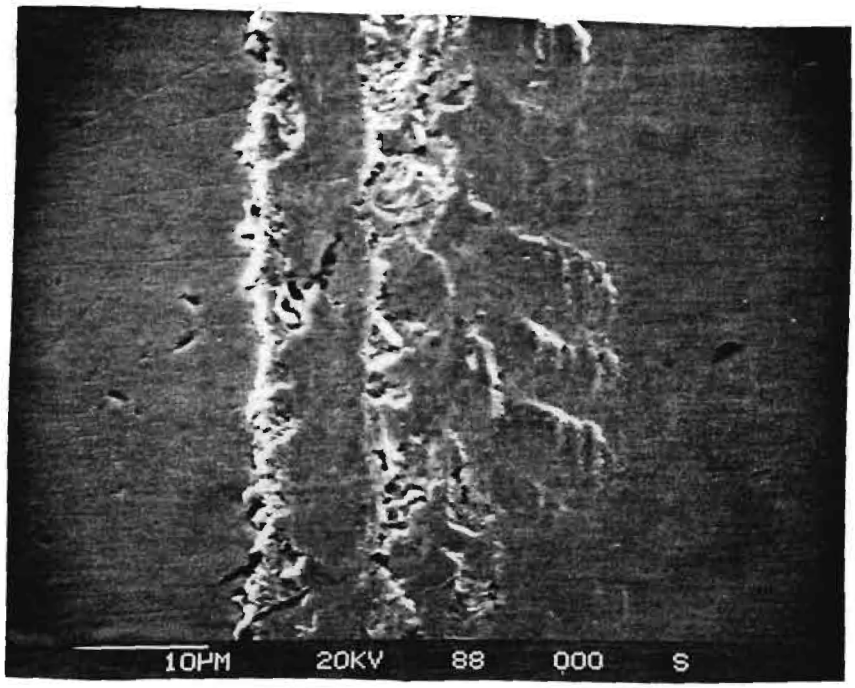

Figure 17. SEM Micrograph of Wear Scar. X2000 Sample 2, Track 2 (See Table 1)

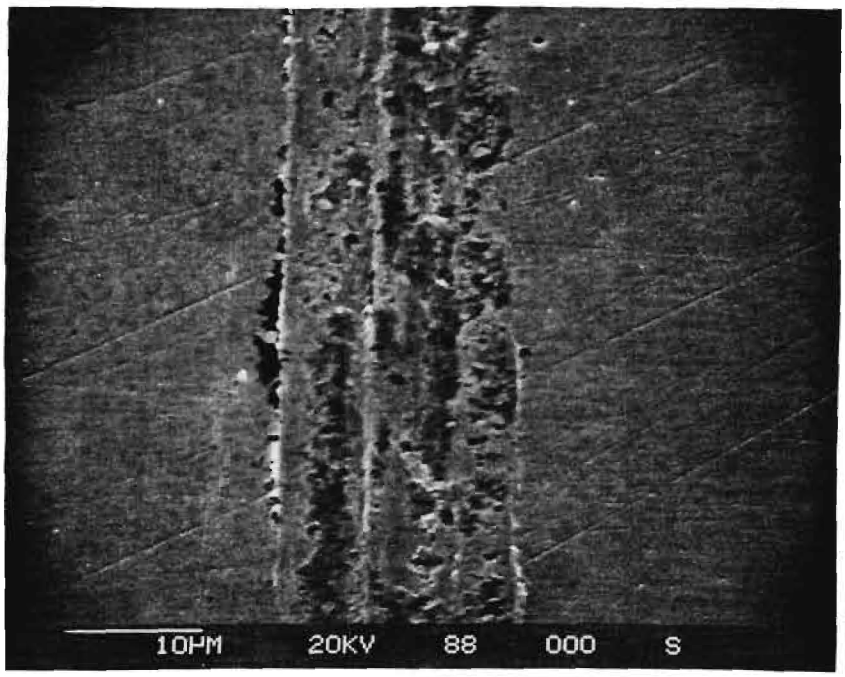

Figure 18. SEM Micrograph of Wear Scar. X2000 Sample 2, Track 3 (See Table 1 for Notation)

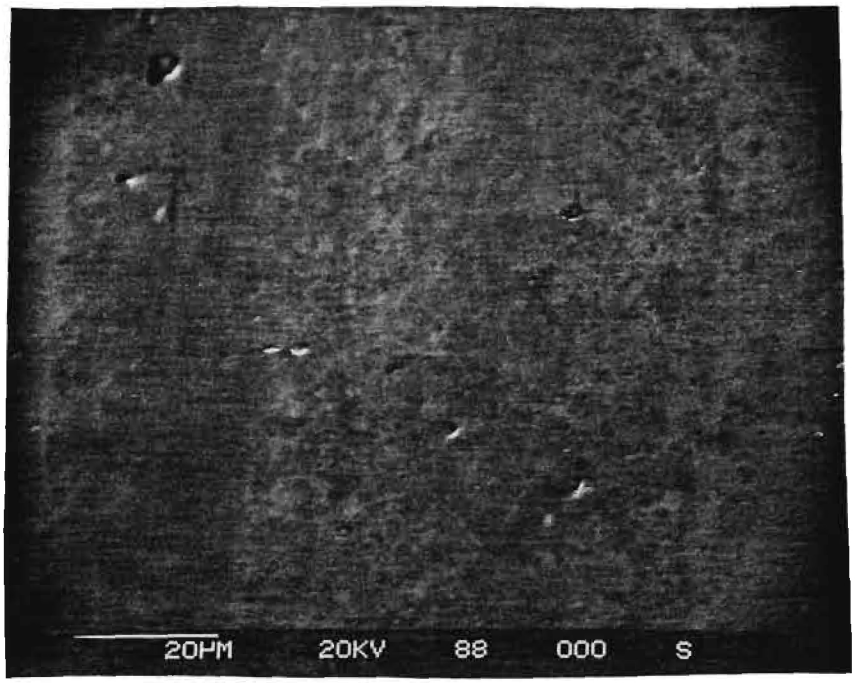

Figure 19. SEM Micrograph of Wear Scar. X1000 Sample 3, Track 1 (See Table 1)

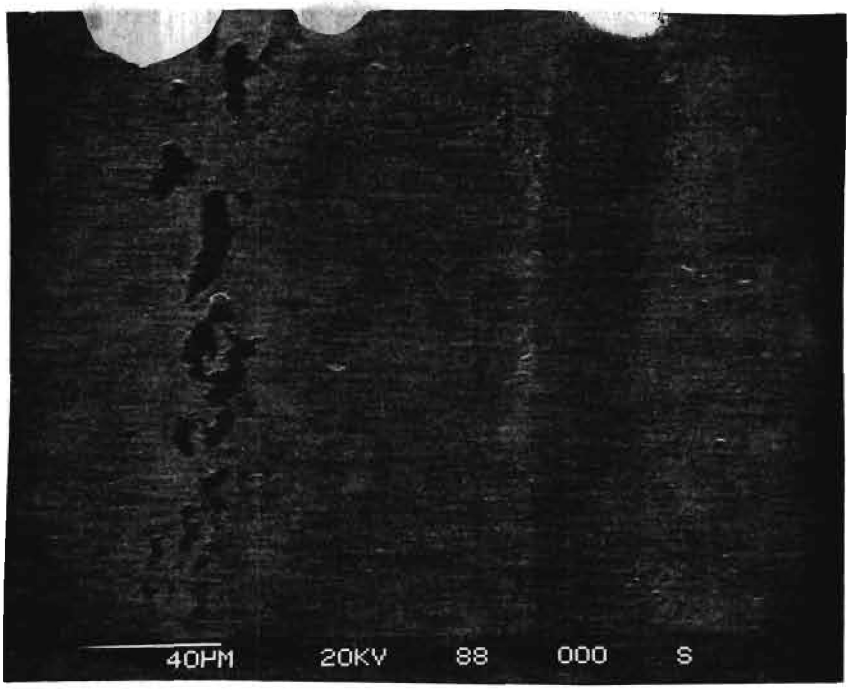

Figure 20. SEM Micrograph of Wear Scar. X500 Sample 3, Track 3 (See Table 1)

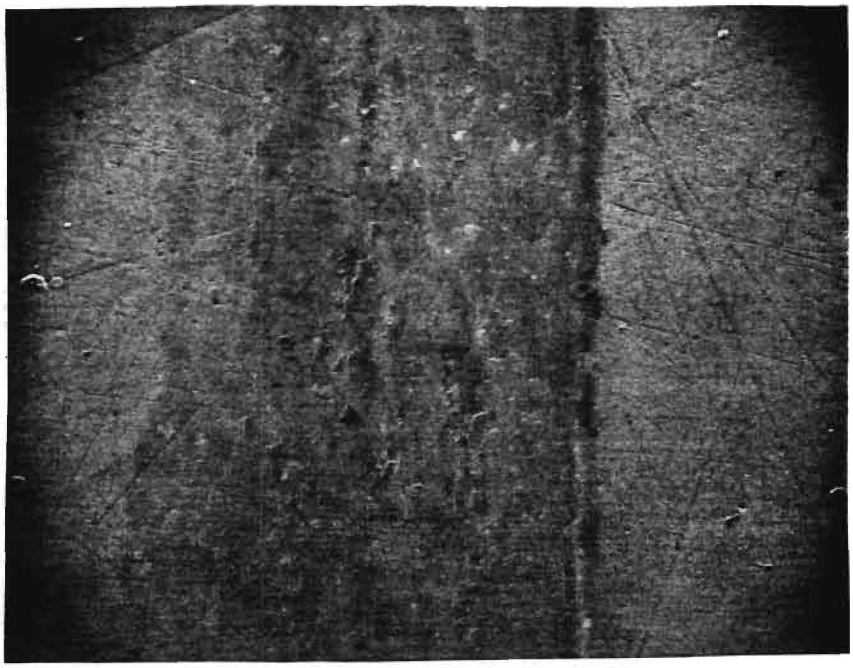

Figure 21. SEM Micrograph of Wear Scar. X2000 Sample 4, Track 1 (See Table 1)

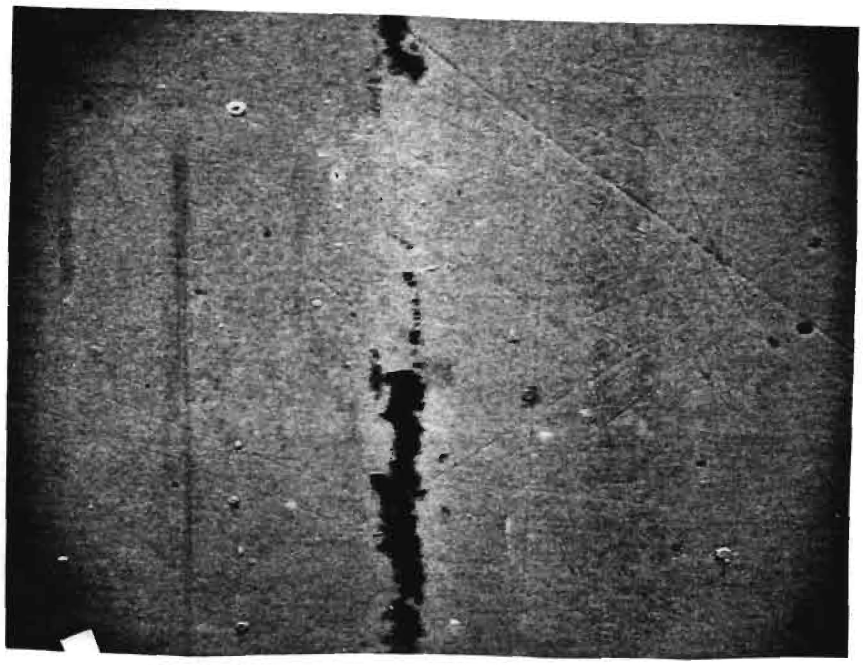

Figure 22. SEM Micrograph of Wear Scar. X1000 Sample 4, Track 3 (See Table 1 for Notation)

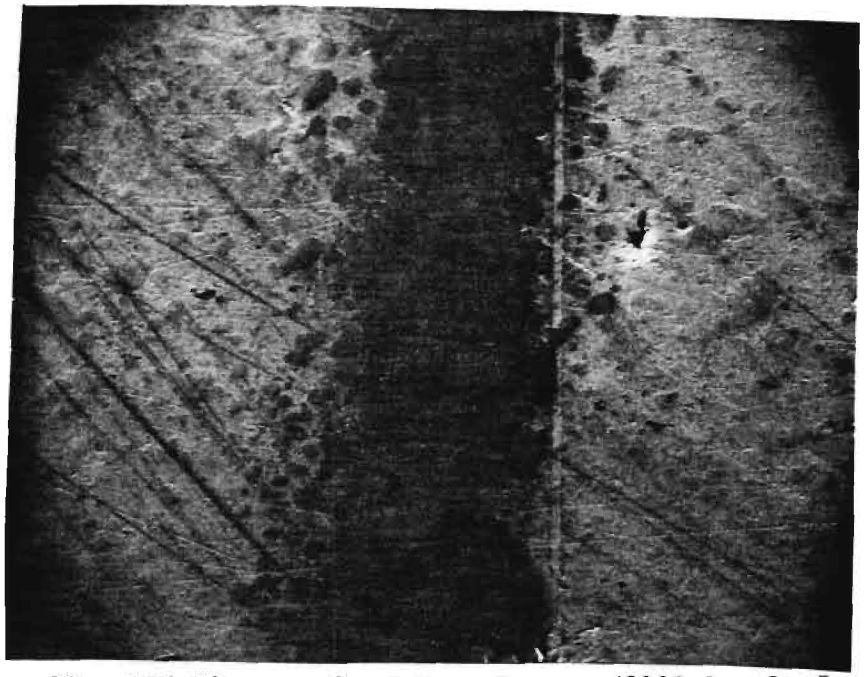

Figure 23. SEM Micrograph of Wear Scar. X2000 Sample 5, Track 1 (See Table 1)

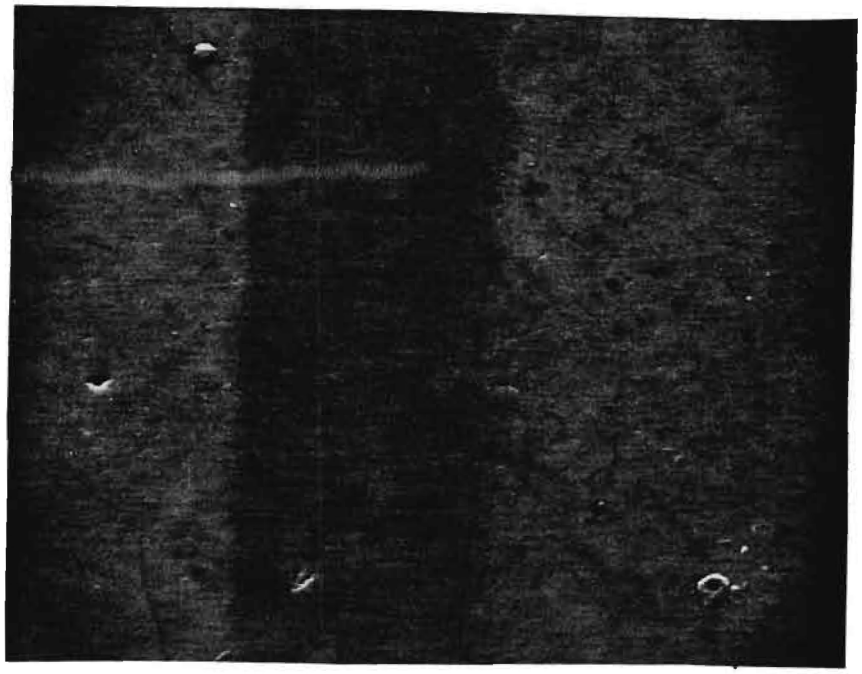

Figure 24. SEM Micrograph of Wear Scar. X2000 Sample 5, Track 2 (See Table 1)

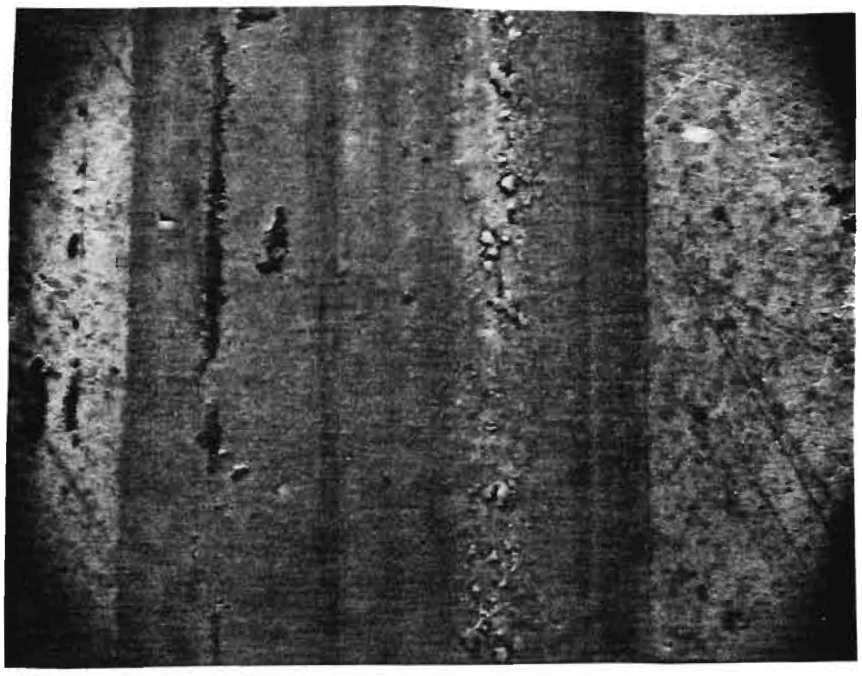

Figure 25. SEM Micrograph Wear Scar. X1000 Sample 5, Track 3 (See Table 1)

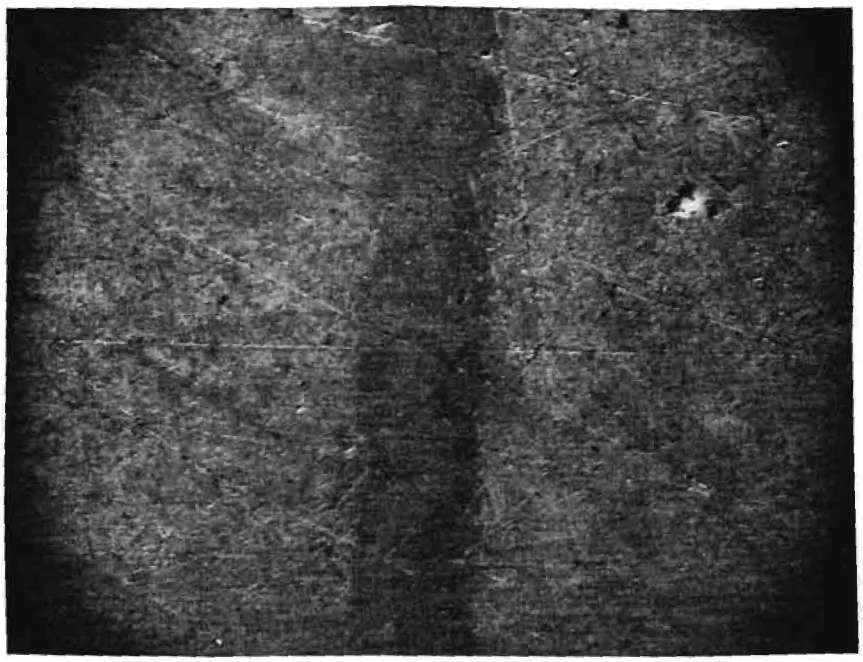

Figure 26. SEM Micrograph of Wear Scar, X2000 Sample 6, Track 1 (See Table 1)

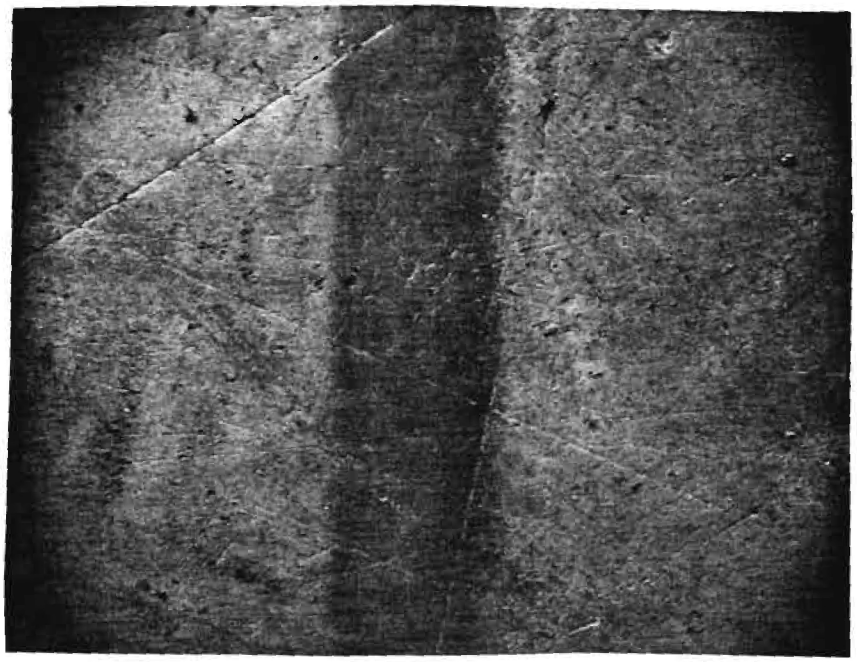

Figure 27. SEM Micrograph of Wear Scar. X2000 Sample 6, Track 2 (See Table 1)

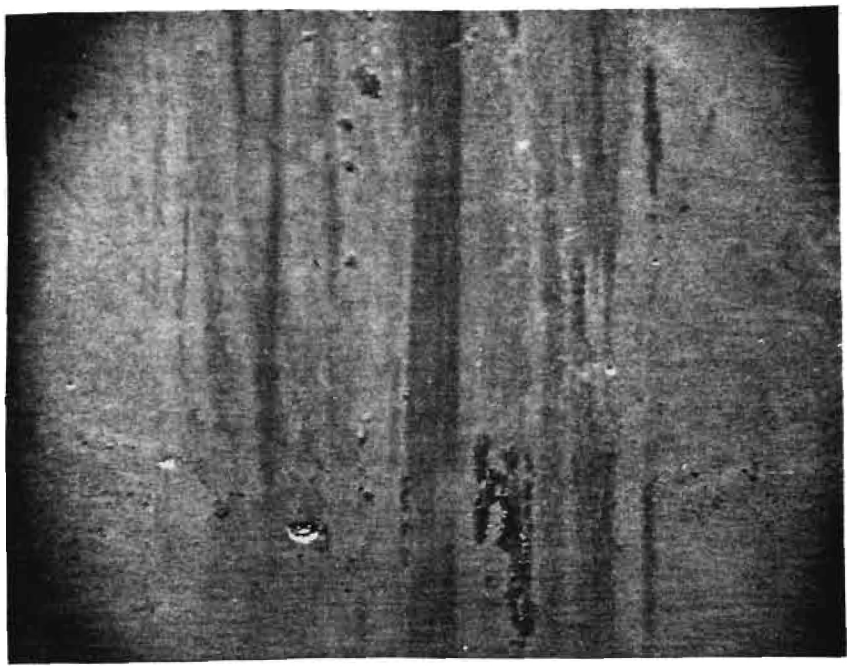

Figure 28. SEM Micrograph of Wear Scar. X500 Sample 6, Track 3 (See Table 1 for Notation)

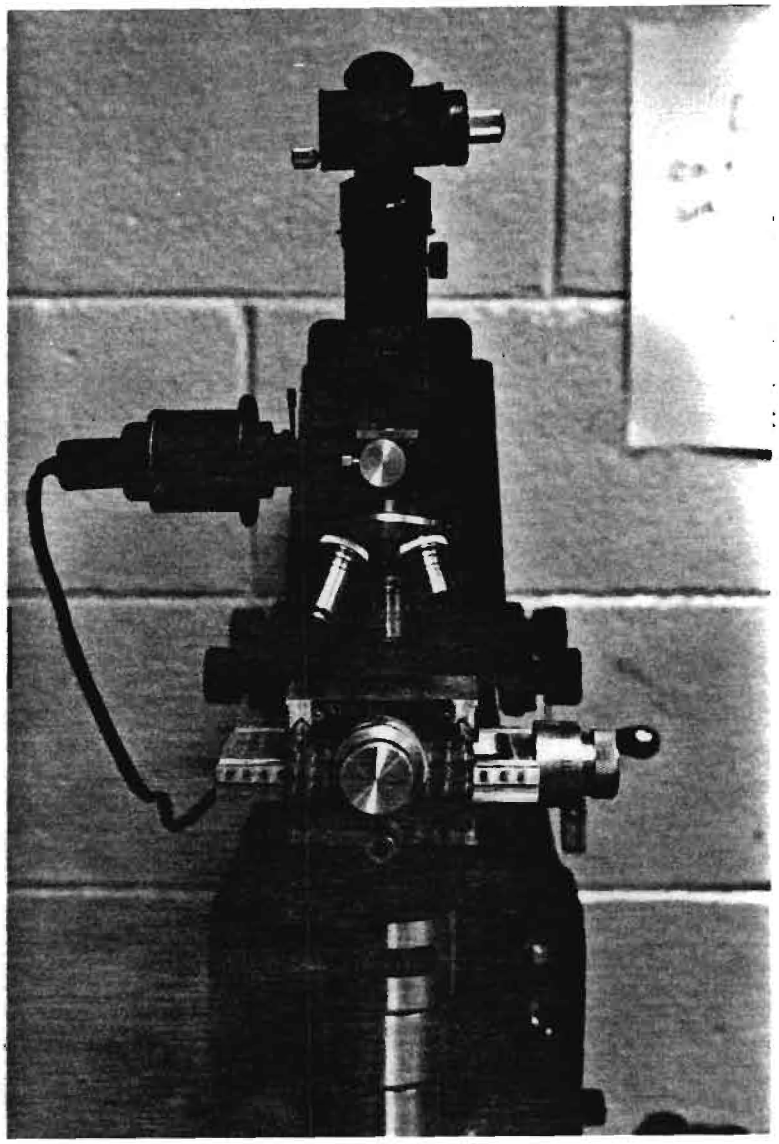

Figure 29. Microhardness Test Machine

Neither a material removal nor a wear depth factor is meaningful for assessing wear damage here. Along a profilometer trace across a wear scar there are areas where the material has been removed and areas where it has been built up. A roughly quantitative damage factor for each track was therefore estimated in terms of the maximum displacements measured with the profilometer. A more precise measurement might be obtained by modifications to the profilometer which would make it possible to automatically step from one trace to the next and conduct a computer aided integration of the wear damage. The damage data obtained here are summarized in Table 1.

Microhardness measurements were carried out with the commercial device shown in Figure 29 and the data are presented in Table 2.

TABLE 1

SUMMARY OF WEAR DAMAGE

Sample	WEAR STRESS			
	Track 1 Sapphire, 50 dyne 108,000 cycles	Track 2 Sapphire, 25 dyne 54,000 cycles	Track 3 304 SS, 50 dyne 54,000 cycles	Track 4 304 SS, 25 dyne 54,000 cycles
(1) 440-C Blank	1KA - 2KA (light scratch with tear in center)	15KA	3KA	Negl.
(2) 52100 Blank	7-15KA	4KA - 5KA	1KA - 1.7KA	Negl.
(3) 440-C TiC Film	Negl. (Visible as dark line only)	Negl. (Visible)	3.5KA - 5KA	3KA
(4) 52100 TiC Film	2.5KA - 10KA	2.5KA	1-2KA	0.7 KA - 2.5 KA (Wide Track)
(5) 440-C TiNi-TiC	25 + KA (Sharp line scratch)	1KA - 1.5 KA (Sharpline)	Negl - 2KA	less than 0.5KA
(6) 52100 TiNi-TiC	Small (Not Visible)	Small (Not Visible)	0.5KA - 2.5KA	1KA - 2.5 KA (Wide Track)

TABLE 2

MICROHARDNESS MEASUREMENTS
500 gram load

Sample	Knoop Hardness Scale	Rockwell C Scale
1	272	21
2	225	13
3	265	20
4	272	21
5	265	20
6	260	18.5

SUMMARY

It is difficult to draw general conclusions based on the small sample size involved here. However, the composite coatings appear to have provided improved protection against abrasion. The sapphire stylus broke through the composite coating of the 440-C sample 5 and made a deep but very narrow scar. This may have been pure chance of a weak spot on the disc surface since the other three wear tracks for this specimen involved very little damage. The friction data is reasonable for the coated specimens, yielding kinetic coefficients in the neighborhood of 0.5. The uncoated specimens had friction coefficients which tended to decrease as the load increased. This behavior has been noted for other free metal-metal friction interactions at corresponding small load values. It is interesting that the lowest coefficient occurred for the 52100 blank material which also had a significantly smaller hardness test value. A specimen of 304 SS was polished and run with the NWC specimens and yielded a friction coefficient of 0.25.

APPENDIX

This appendix contains some of the friction curves and profilometer traces made on the wear specimens. The friction curves were made with a traverse speed of 6.5×10^{-4} cm/sec. The data were recorded using an X-Y plotter with the upper curve for motion in one direction and the lower curve for motion in the other direction. Obviously the sign of the friction force switches with traverse direction. The apparatus employed here was designed and built at Georgia Tech.

The profilometer traces were made using a commercial device made by Tencor Instruments, "Alpha-Step Model 10-0030, 0020. All the traces shown were made with a horizontal amplification factor of X500. The notation employed on these raw data are: S1 or S2, etc indicates Sample 1 or Sample 2, etc.

Sample 1 was a blank 440-C disc
Sample 2 was a blank 52100 disc
Sample 3 was a 440-C disc coated with 2200Å TiC
Sample 4 was a 52100 disc coated with 2200Å TiC
Sample 5 was a 440-C disc coated with 2200Å TiNi and then 1400Å TiC
Sample 6 was a 52100 disc coated with 2200Å TiNi and then 1400Å TiC

Tk 1, etc indicates "Track 1", etc where

Track 1 is for sapphire stylus at 50 dyne for 108,000 cycles
Track 2 is for sapphire stylus at 25 dyne for 54,000 cycles
Track 3 is for SS stylus at 50 dyne for 54,000 cycles
and Track 4 is for SS stylus at 25 dyne for 54,000 cycles

Tr 1, etc indicates a profile trace perpendicular to a particular wear track at some location.

5KÅ means full scale 5000Å, etc.

A downward deflection indicates a depression in the specimen surface.

0.1 %/in

2nd Trace Track 1

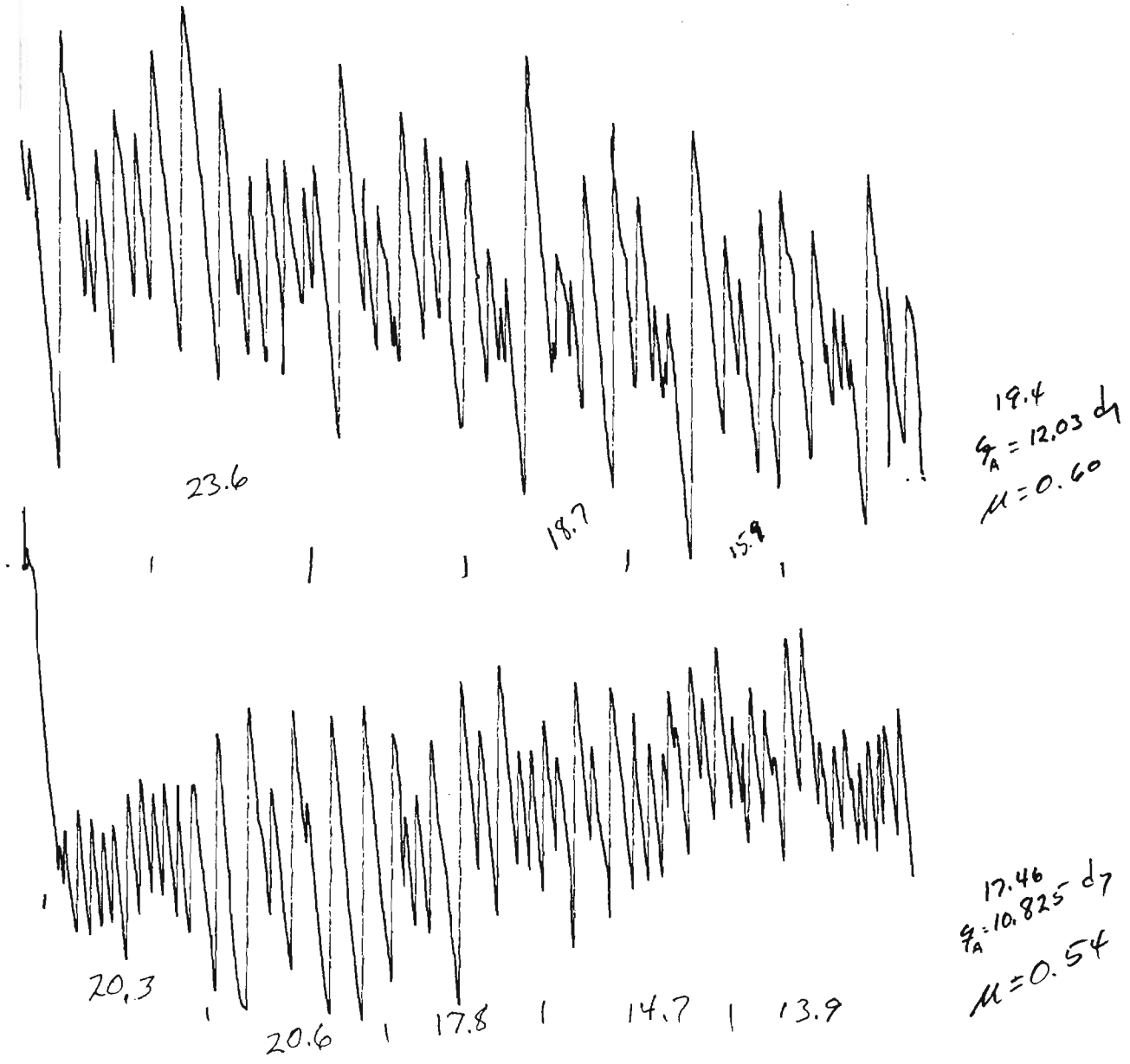

0.2 %

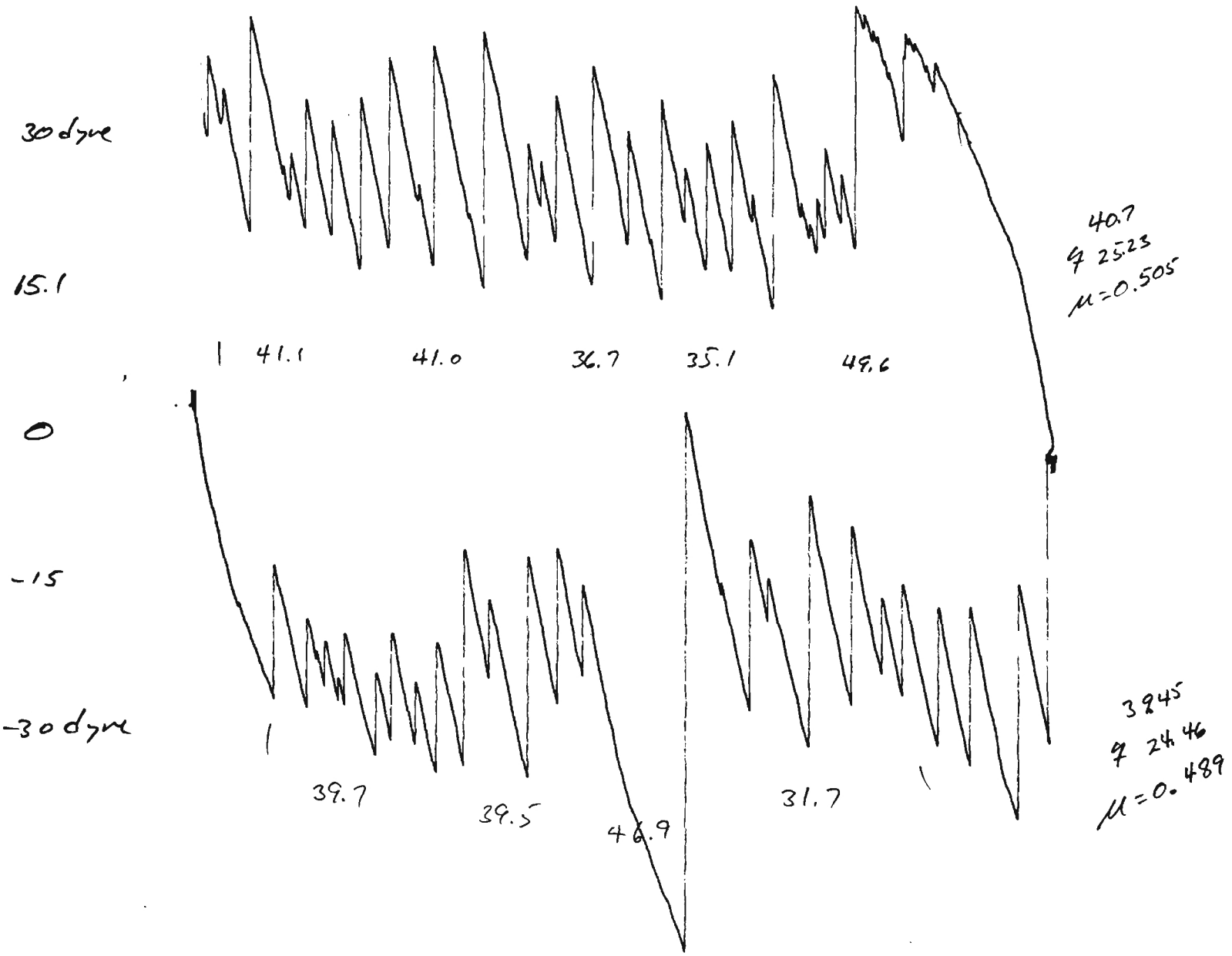
30 dyne
15.1
0
-15
-30 dyne
41.1
41.0
36.7
35.1
49.6
40.7
$\bar{q}$ 25.23
μ=0.505
39.7
39.5
46.9
31.7
39.45
$\bar{q}$ 24.46
μ=0.489

SAMPLE1

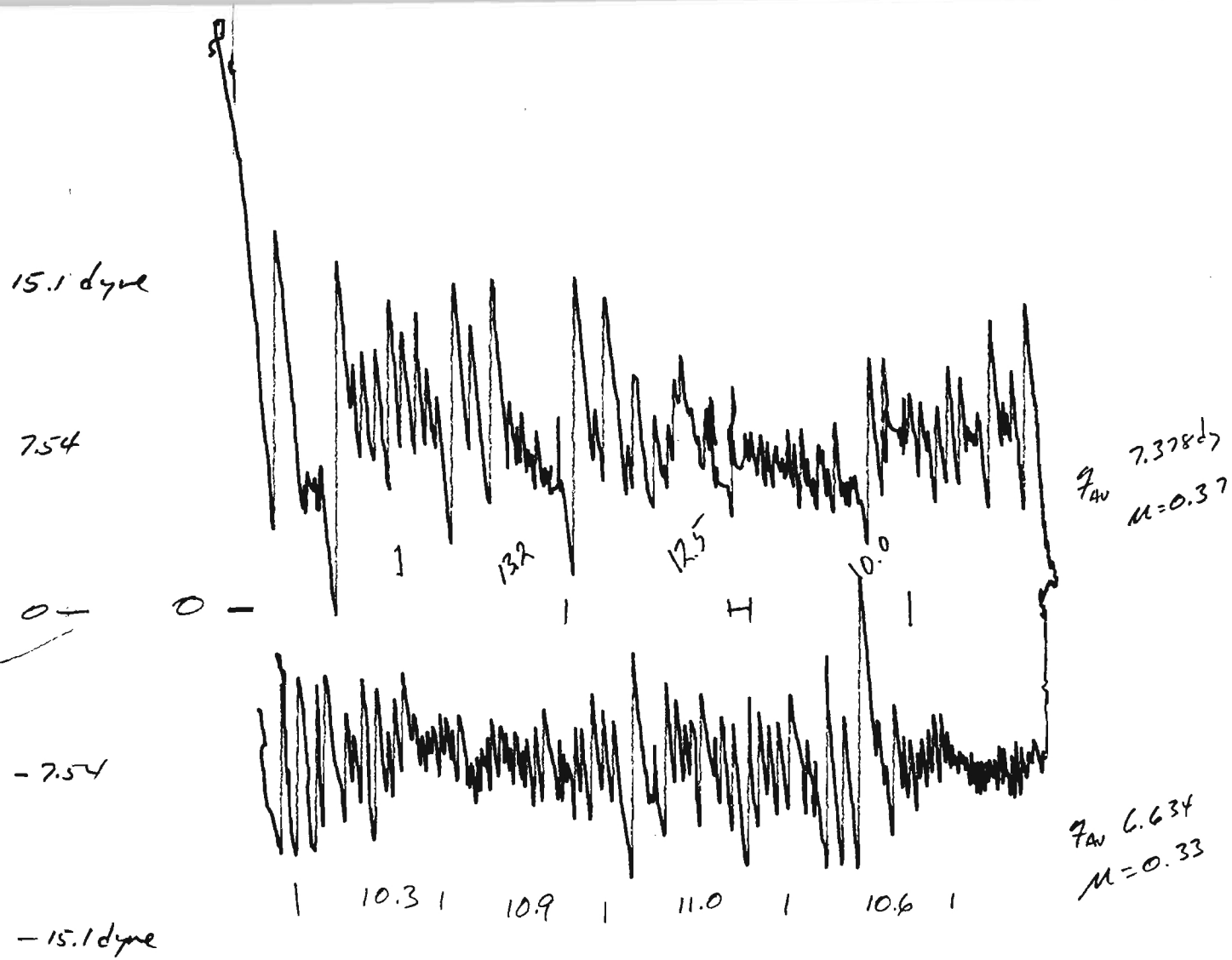
0.1 V/in
15.1 dyne
7.54
0
0
-7.54
-15.1 dyne
1
13.2
12.5
10.0
10.3
10.9
11.0
10.6
η_{AV} 7.378
μ=0.37
η_{AV} 6.634
μ=0.33

SAMPLE 2

.2 V/in

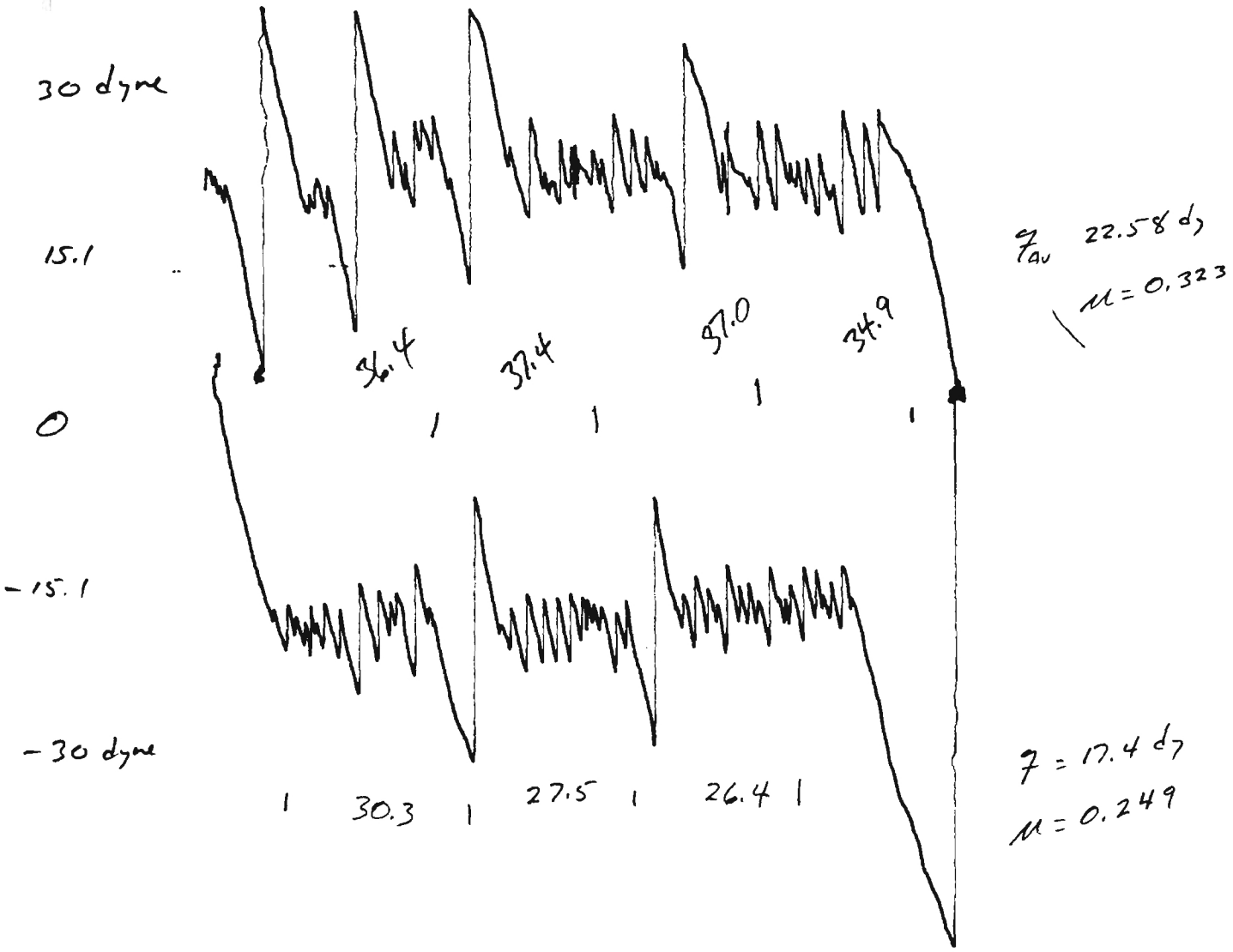

SAMPLE2

SAMPLE 3

Two Normal Force Values
10 dyne
and 50 dyne

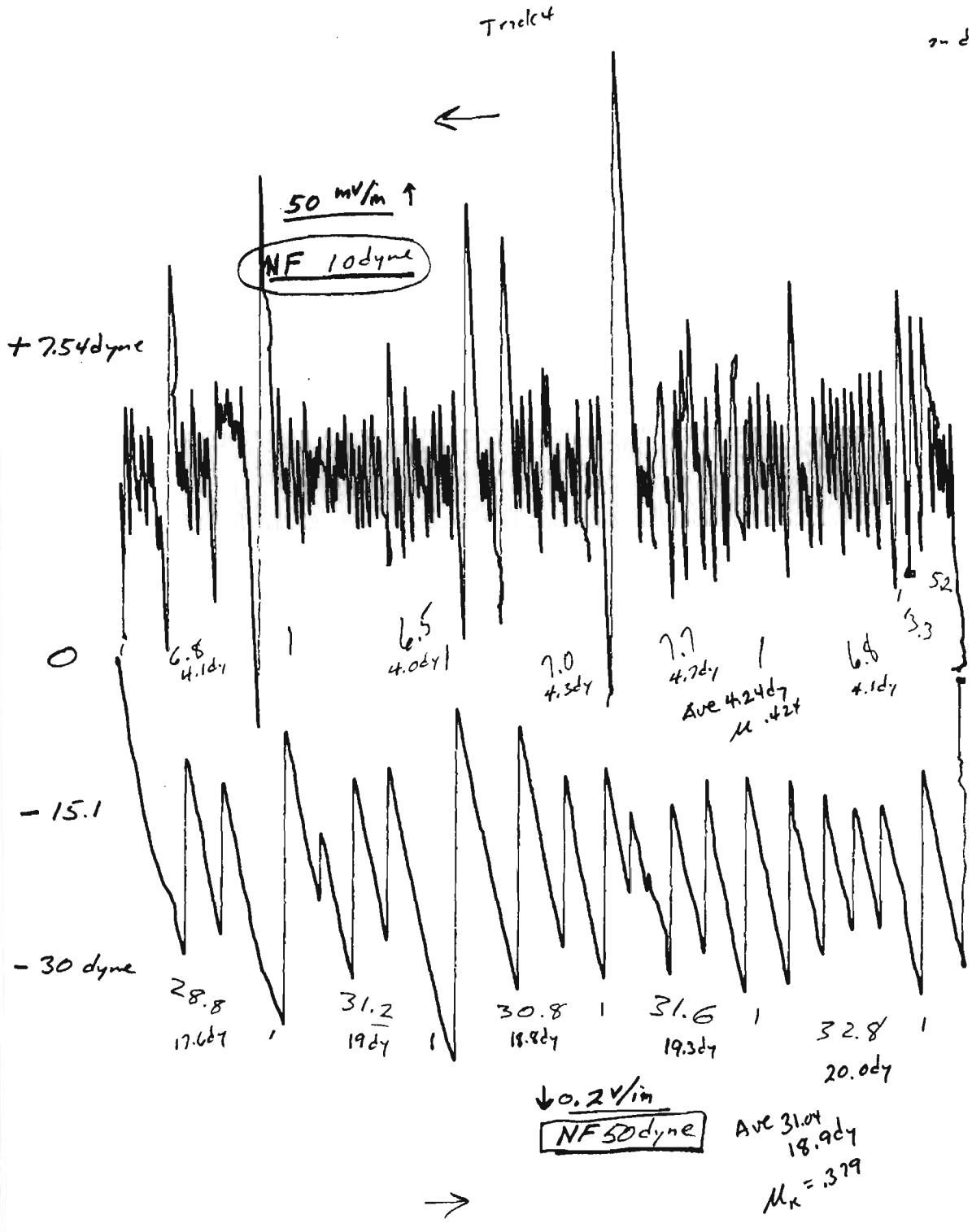

$\bar{q}$ 4.31 dy
μ = 0.431

$\bar{q}_{AV}$ 19.24 dy
μ = 0.38

NF 20 dyne
0.1 V/in

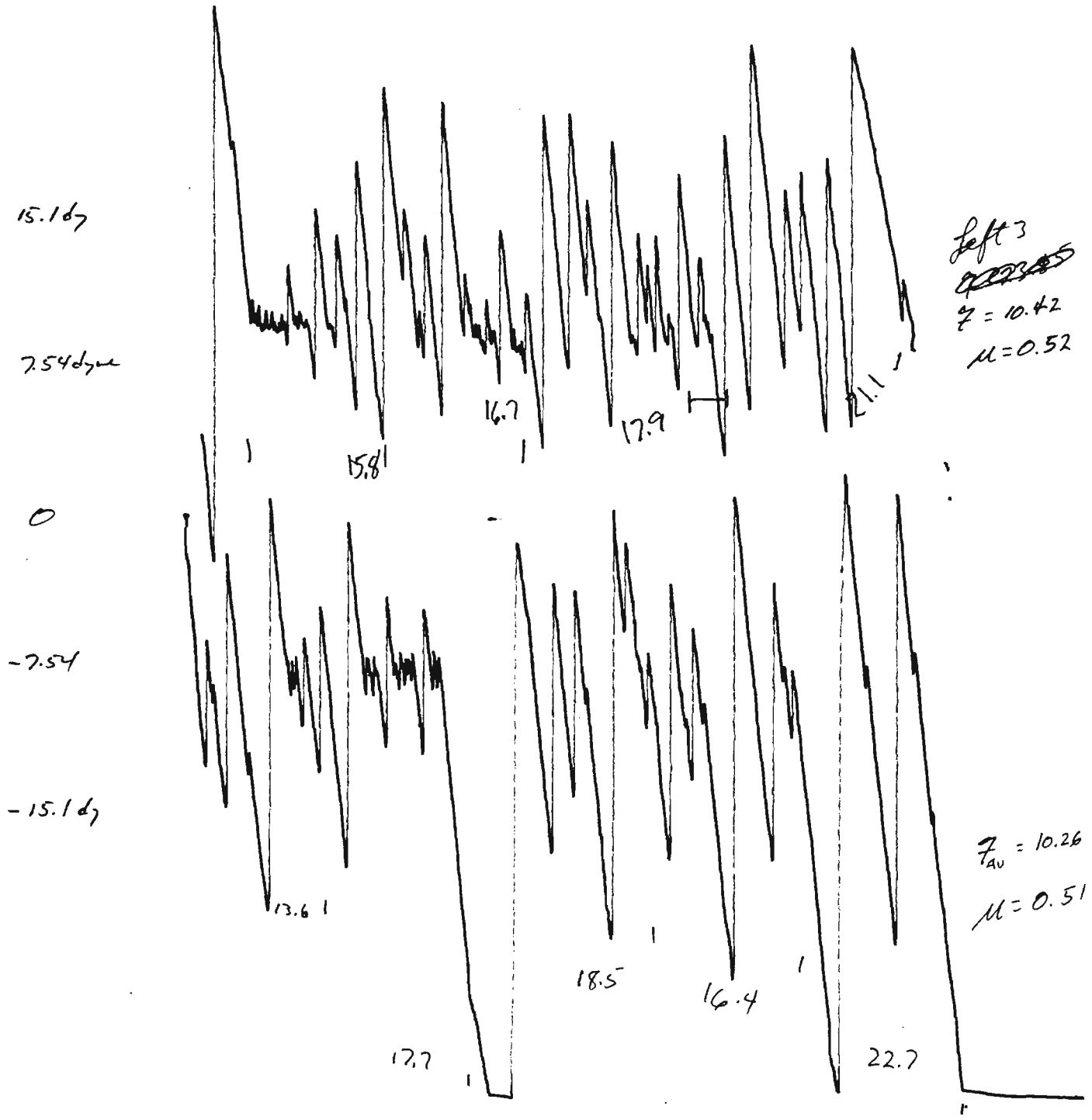

SAMPLE 4

SAMPLE 5
N.F. = 20dyne
First Trace

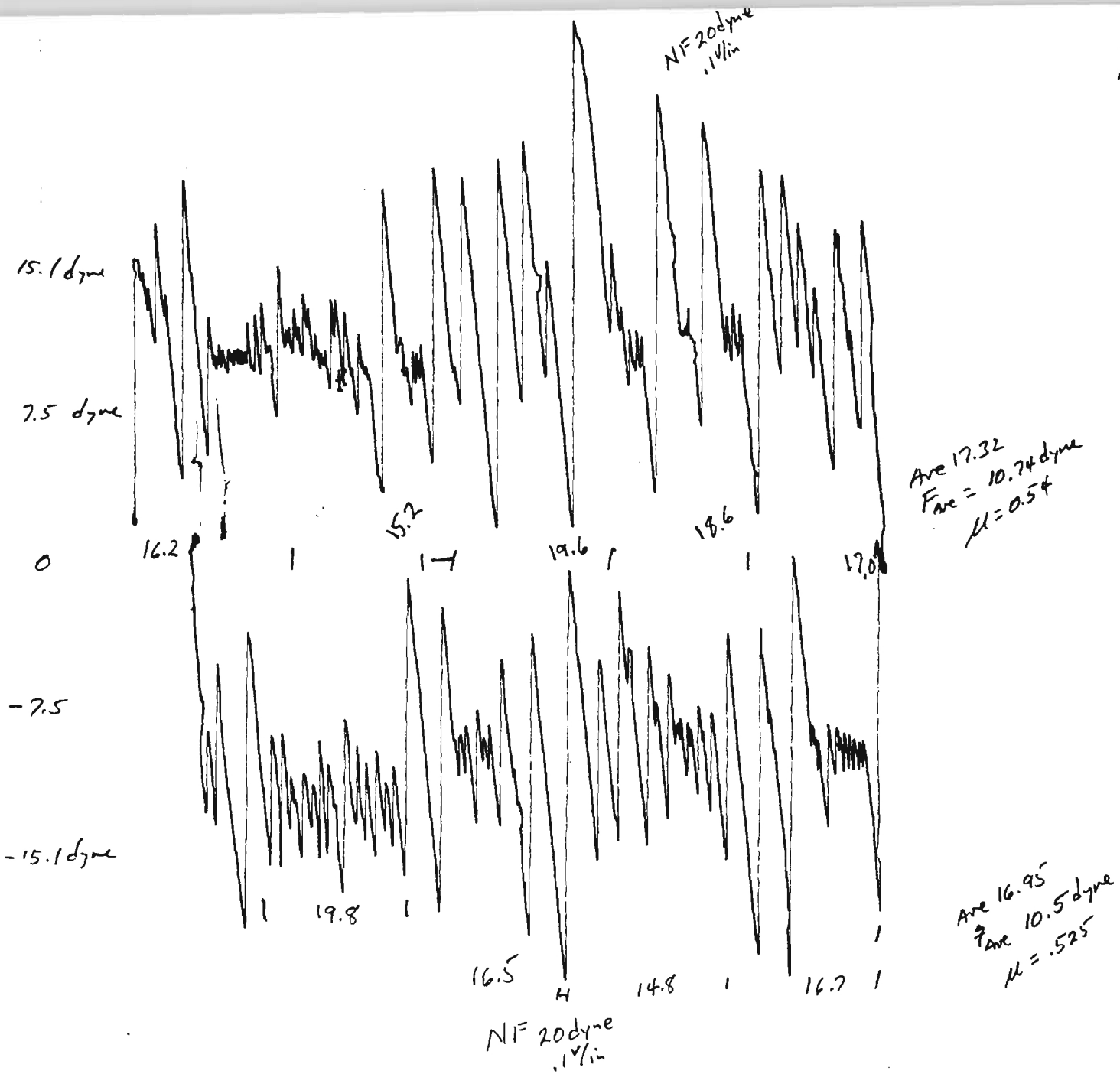

Ave 17.32
F_{Ave} = 10.74 dyne
μ = 0.54

Ave 16.95
F_{Ave} 10.5 dyne
μ = .525

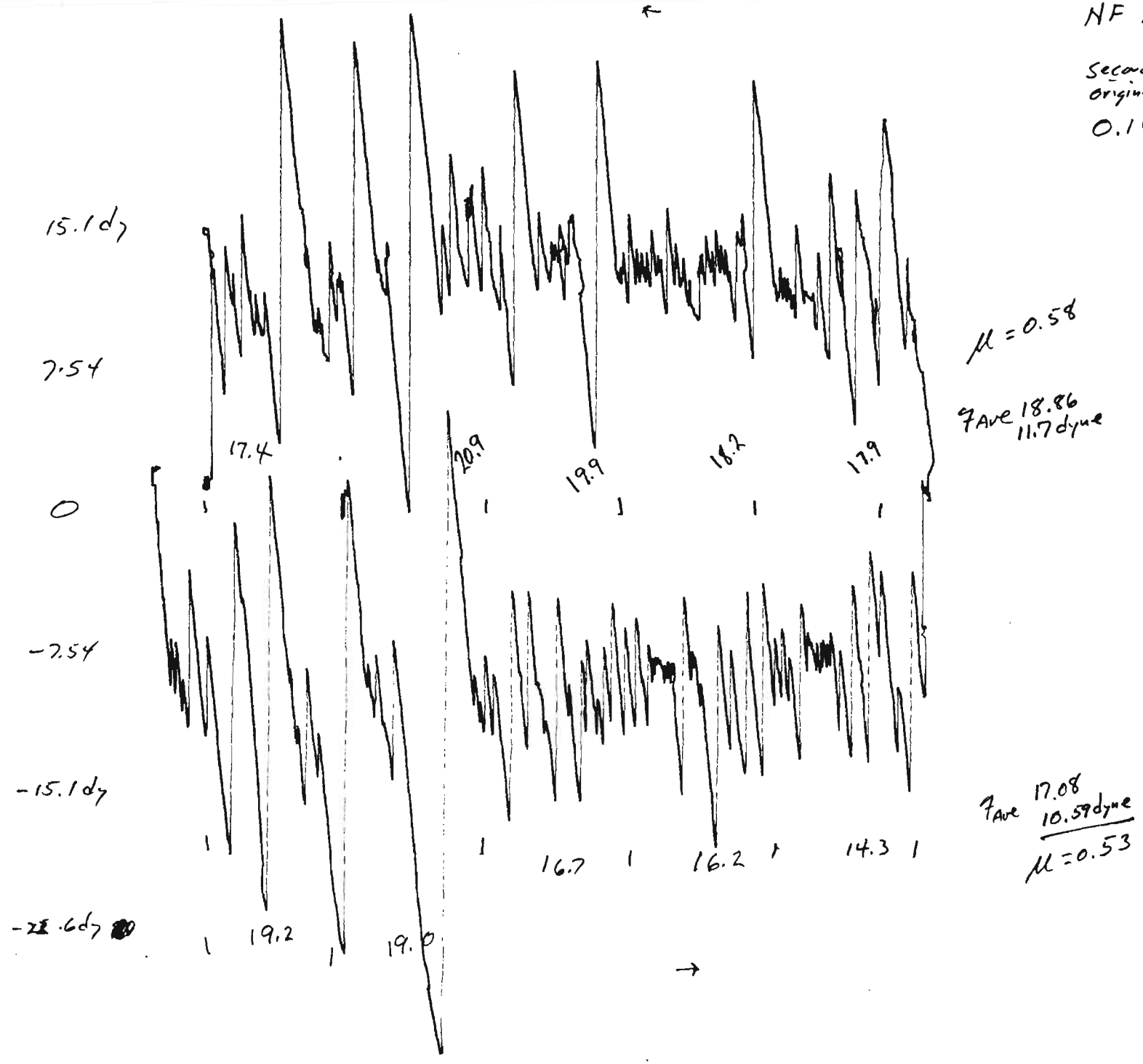
NF 20 dyne
Second trace over original path
0.1 V/in
15.1 dy
7.54
0
-7.54
-15.1 dy
-22.6 dy
17.4
20.9
19.9
18.2
17.9
19.2
19.0
16.7
16.2
14.3
μ = 0.58
τAve 18.86
11.7 dyne
τAve 17.08
10.59 dyne
μ = 0.53

SAMPLES

NF 50 dyne

0.2 V/in Track 2

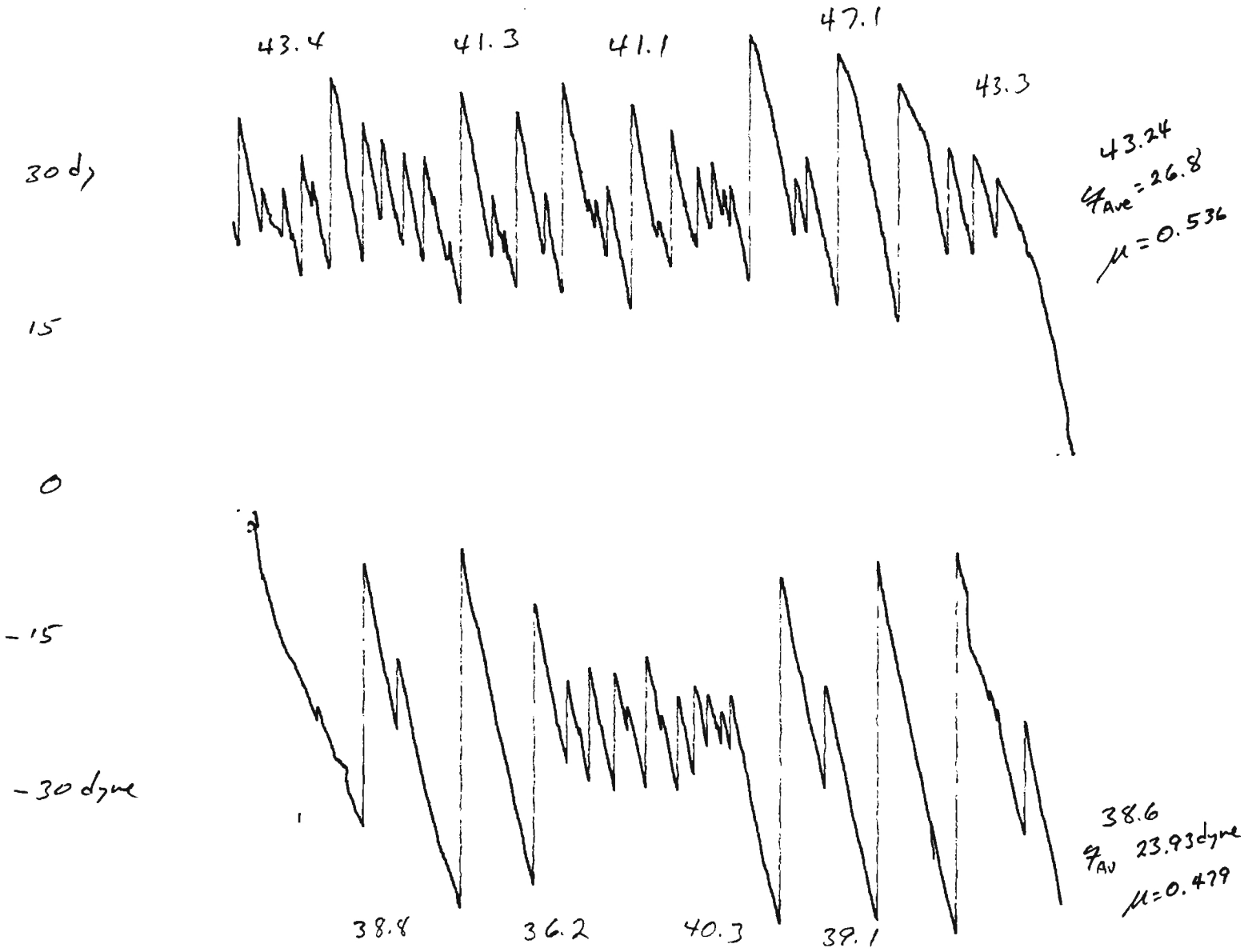

SAMPLES

NF 20dyne

0.1%; Track 2 (After 100dyne tracks)

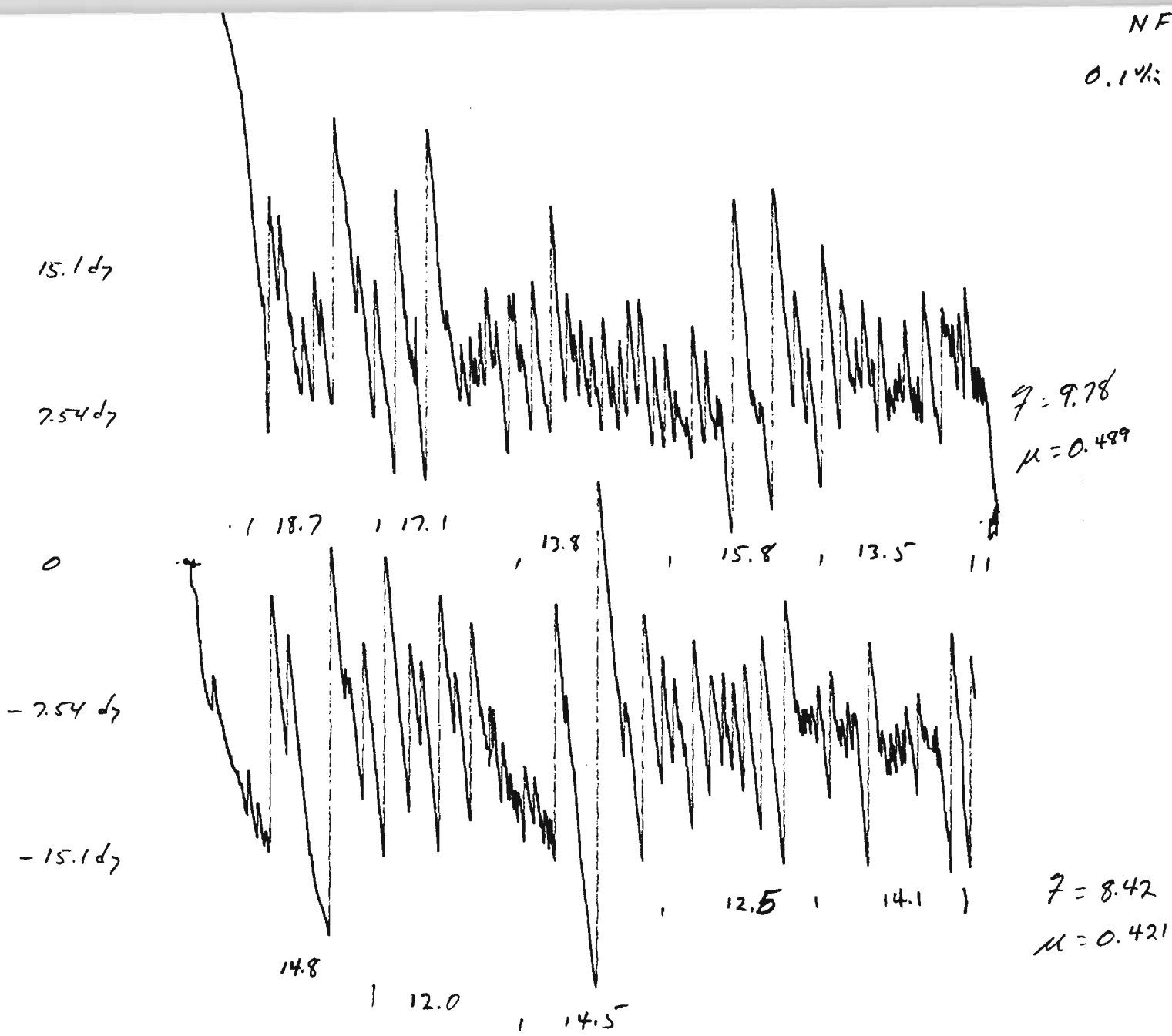

SAMPLE

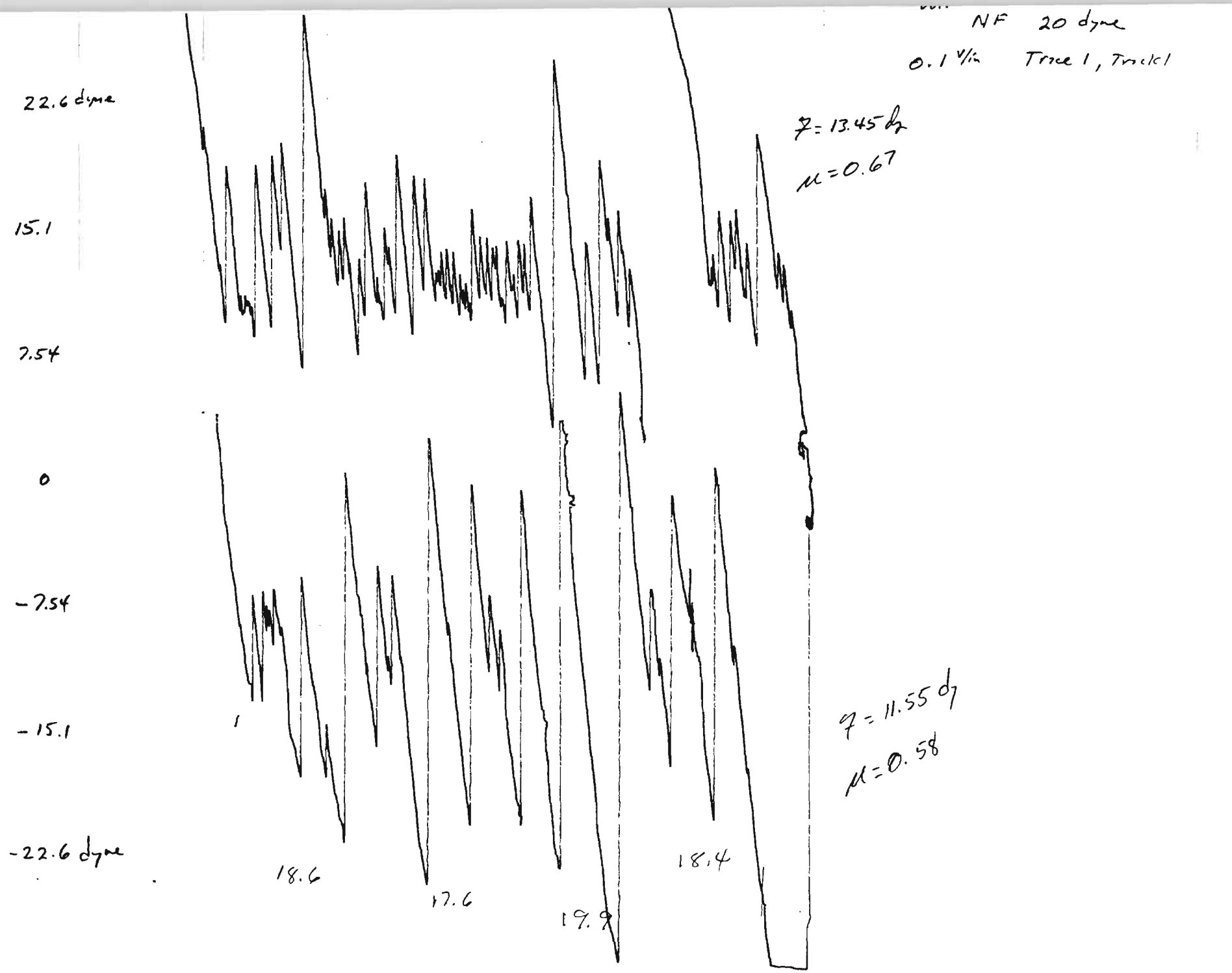
NF 20 dyne
0.1 V/in Trace 1, Track 1
22.6 dyne
15.1
7.54
0
-7.54
-15.1
-22.6 dyne
f = 13.45 dy
μ = 0.67
f = 11.55 dy
μ = 0.58
18.6
17.6
19.9
18.4

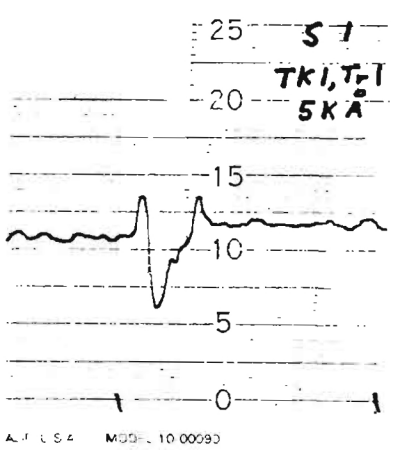
S 1
TK1, Tr1
5 KÅ
25
20
15
10
5
0

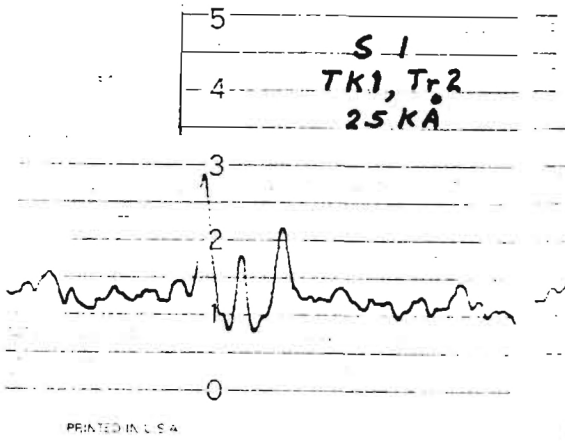
S 1
TK1, Tr2
2.5 KÅ
5
4
3
2
1
0

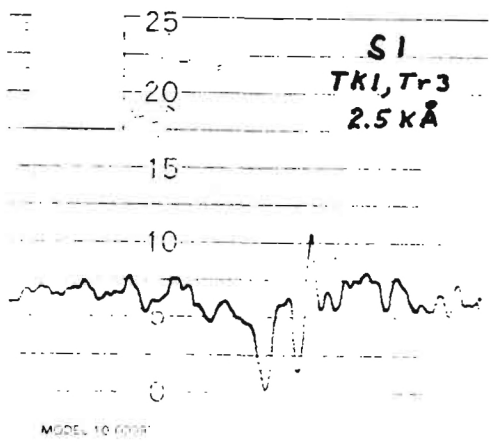
S 1
TK1, Tr3
2.5 KÅ
25
20
15
10
5
0

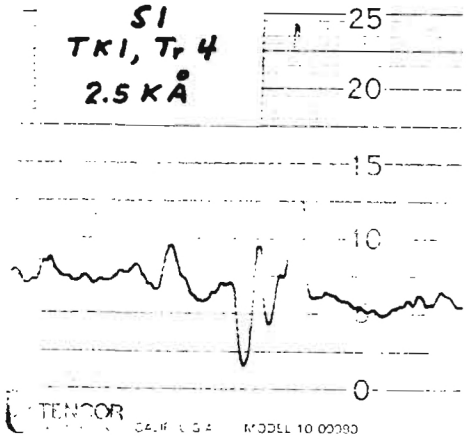
S1
TK1, Tr 4
2.5 KÅ
25
20
15
10
0
TENCOR

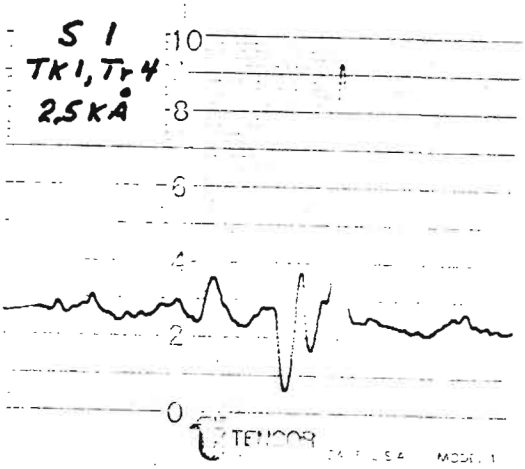
S 1
TK1, Tr 4
2.5 KÅ
10
8
6
4
2
0
TENCOR

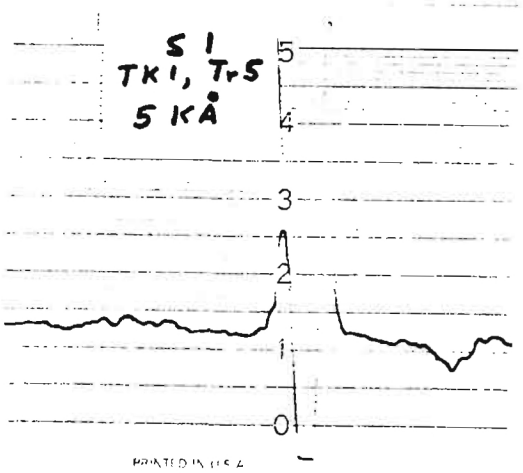
S 1
TK1, Tr5
5 KÅ
5
4
3
2
1
0

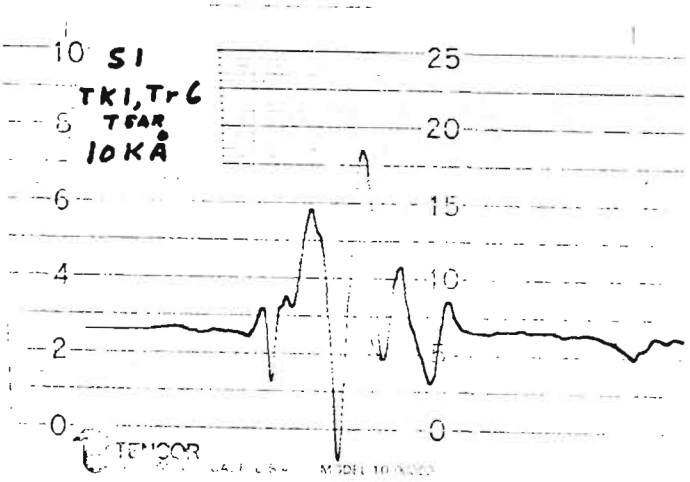
S1
TK1, Tr6
TEAR
10 KÅ
10
8
6
4
2
0
25
20
15
10
0
TENCOR

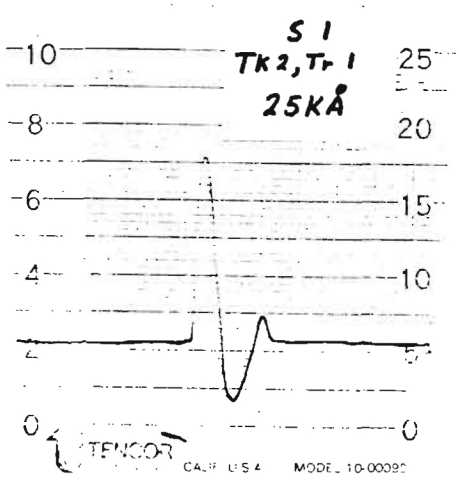
S1
TK2, Tr1
25KÅ
TENCOR

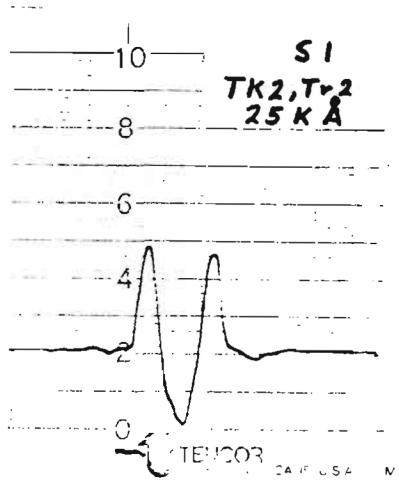
S1
TK2, Tr2
25 KÅ
TENCOR

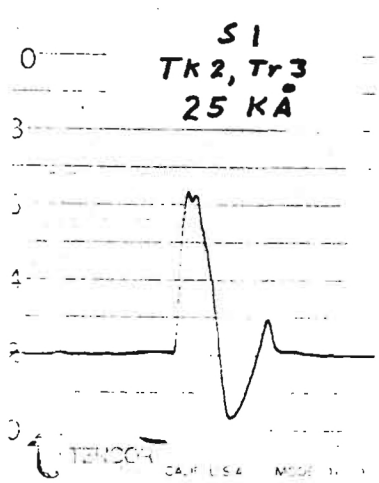
S1
TK2, Tr3
25 KÅ
TENCOR

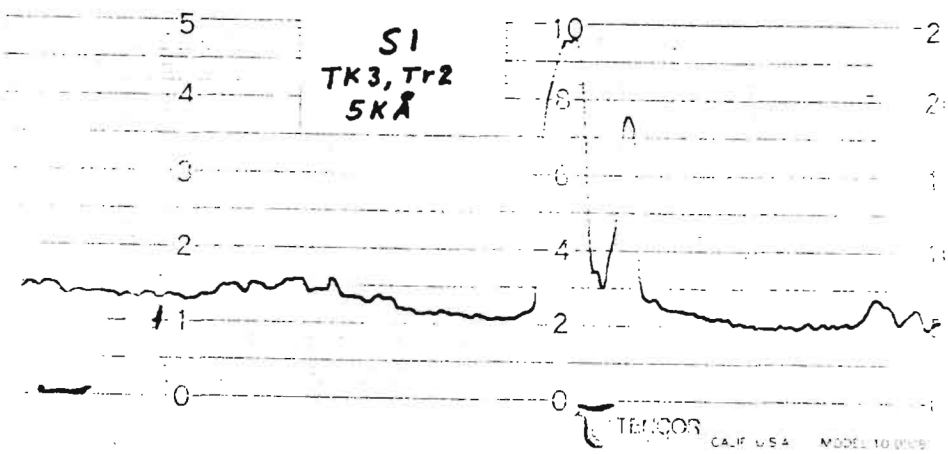
S1
TK3, Tr2
5KÅ
TENCOR

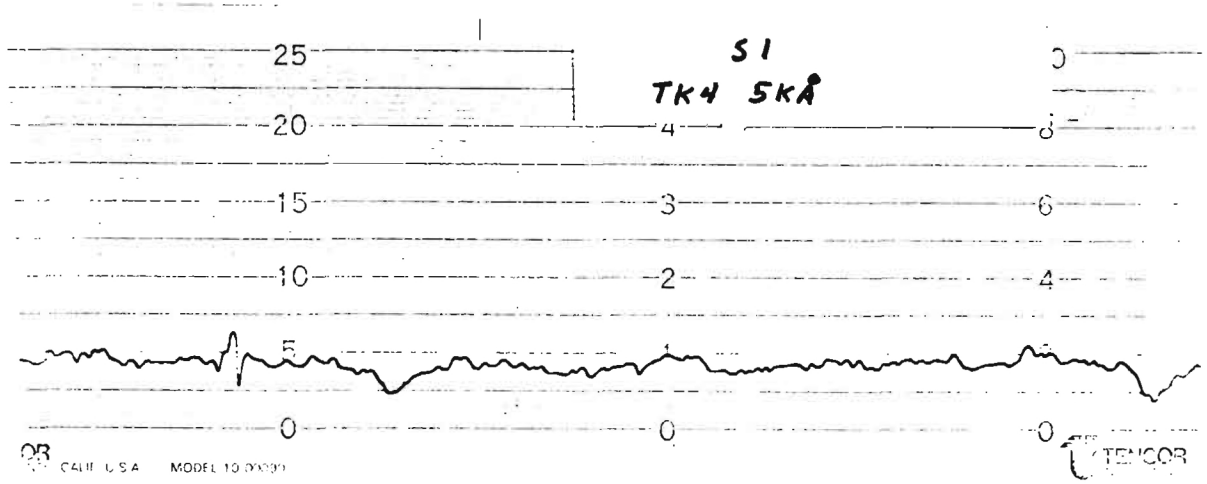
S1
TK4 5KÅ
TENCOR

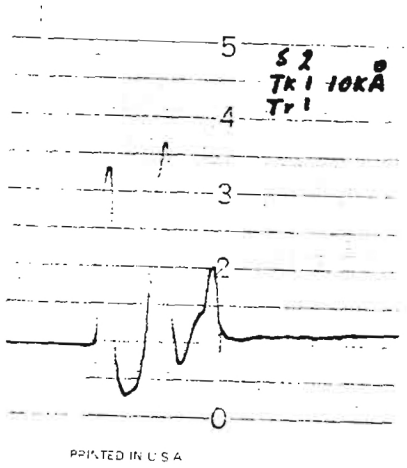

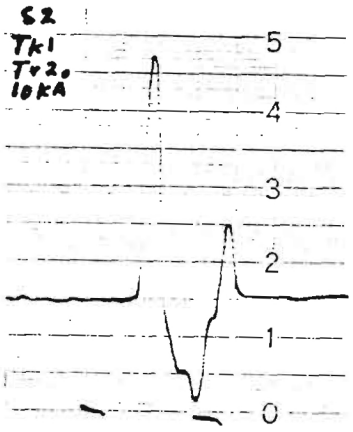

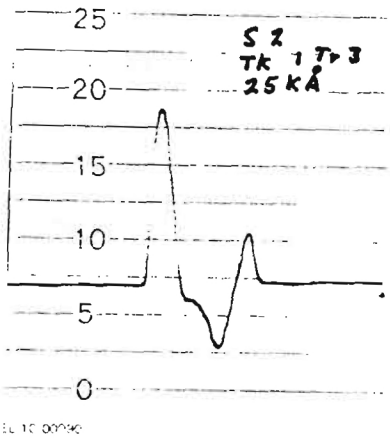

PRINTED IN U.S.A.

EL 10 00090

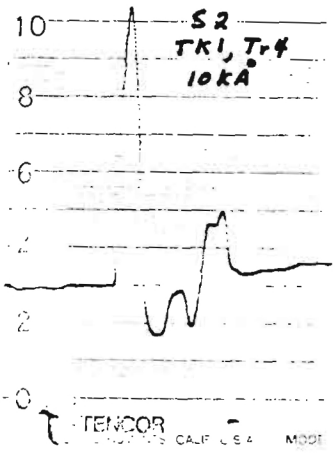

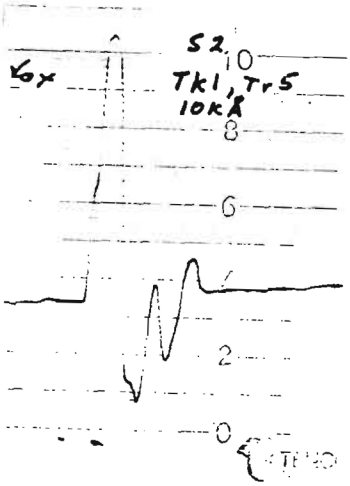

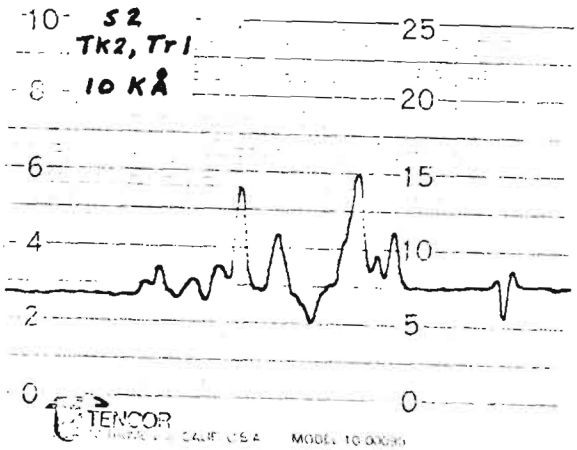

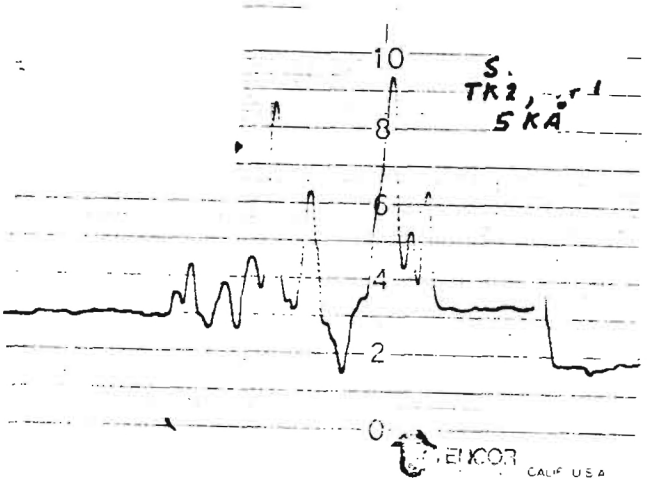
10
8
6
4
2
0
S
TK2, Tr 1
5KÅ
ELKCOR
CALIF USA

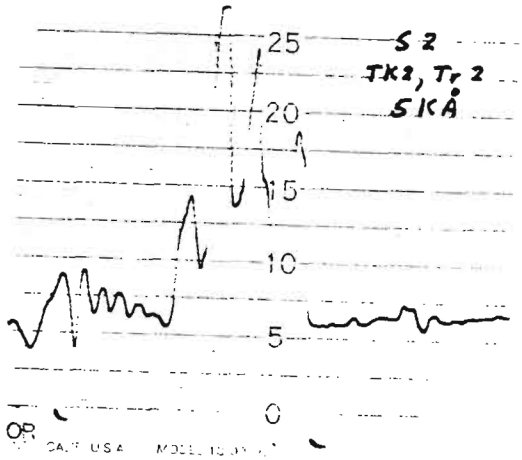
25
20
15
10
5
0
S 2
TK2, Tr 2
5KÅ
CALIF USA

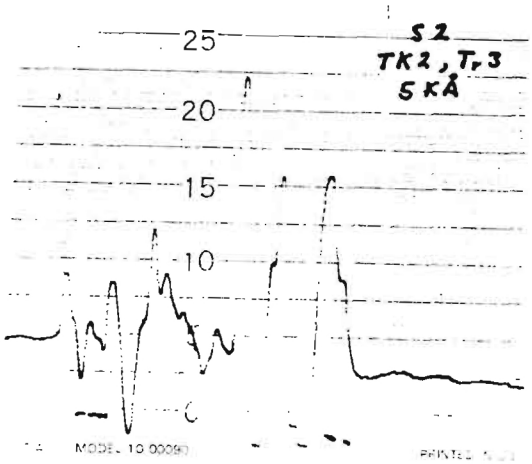
25
20
15
10
0
S 2
TK2, Tr 3
5KÅ

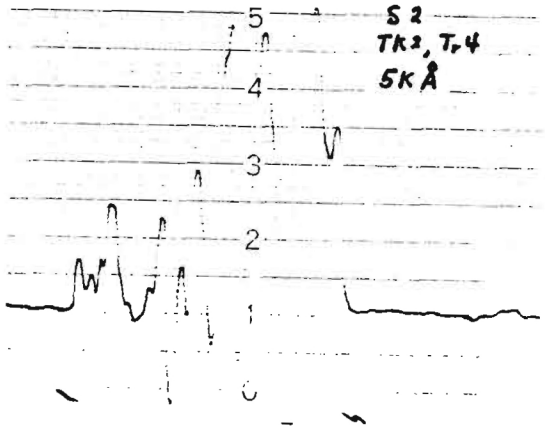
5
4
3
2
1
0
S 2
TK2, Tr 4
5KÅ

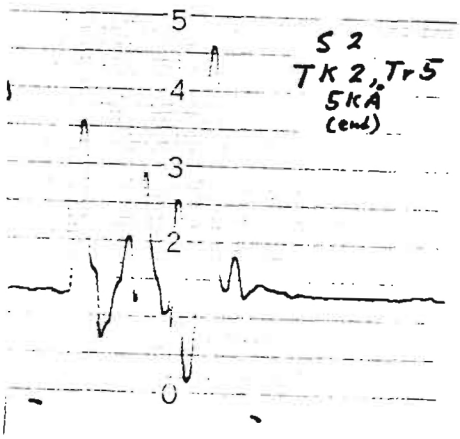
5
4
3
2
1
0
S 2
TK 2, Tr 5
5KÅ
(end)

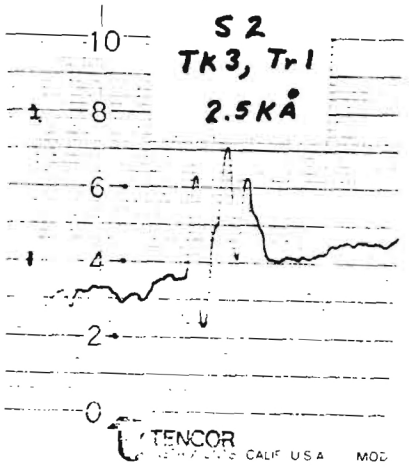
S 2
Tk 3, Tr 1
2.5 kÅ
10
8
6
4
2
0
TENCOR

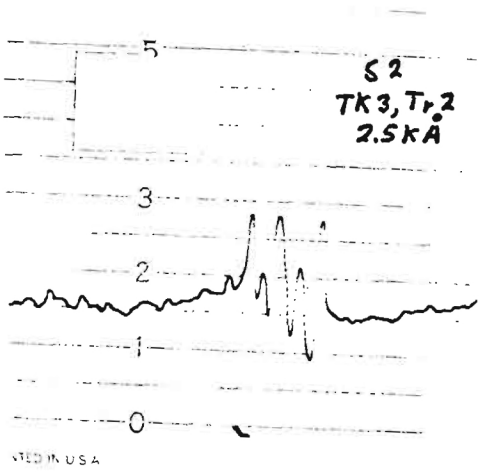
S 2
Tk 3, Tr 2
2.5 kÅ
5
3
2
1
0

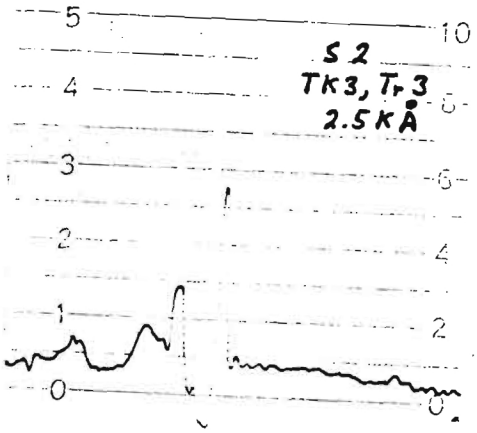
S 2
Tk 3, Tr 3
2.5 kÅ
5
4
3
2
1
0
10
8
6
4
2
0

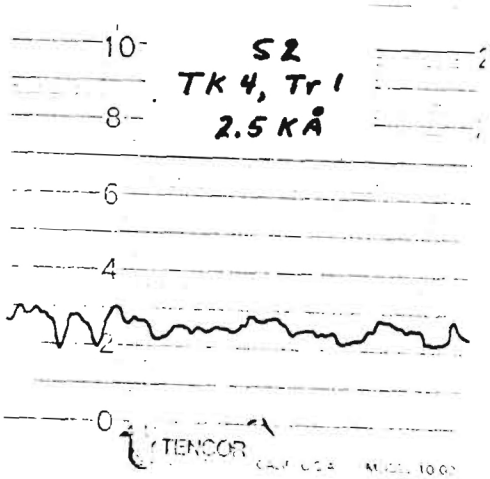
S 2
Tk 4, Tr 1
2.5 kÅ
10
8
6
4
2
0
TENCOR

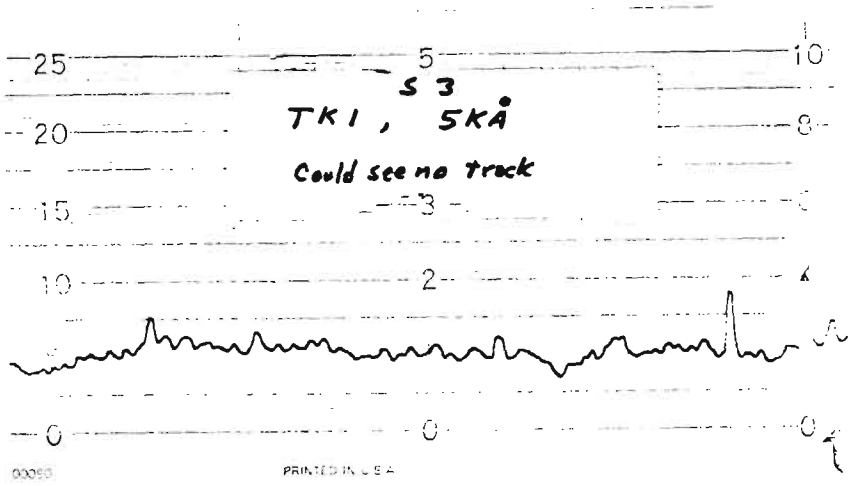
S 3
TK 1, 5KÅ
Could see no track
PRINTED IN U.S.A.

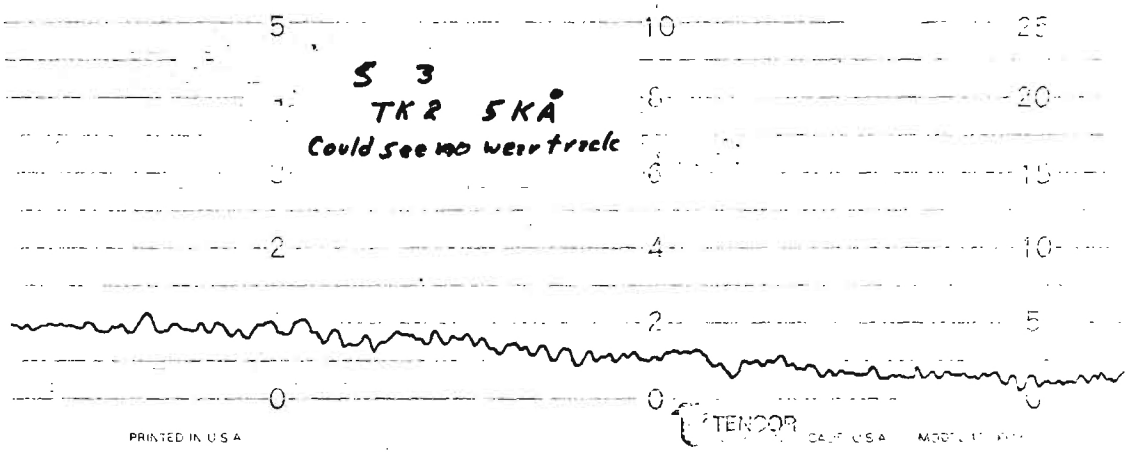
S 3
TK 2 5KÅ
Could see no wear track
PRINTED IN U.S.A.
TENCOR

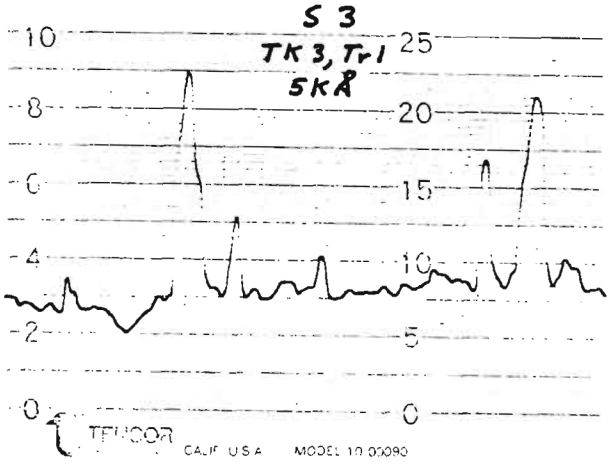
S 3
TK 3, Tr 1
5KÅ
10
8
6
4
2
0
25
20
15
10
5
0
TEKCOR
CALIF U.S.A.
MODEL 10 00090

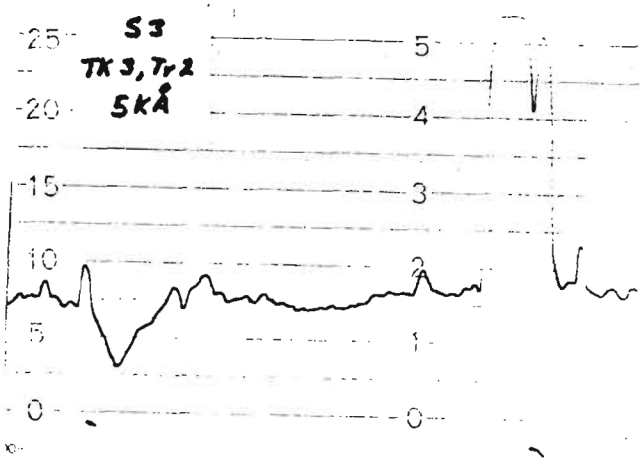
S 3
TK 3, Tr 2
5KÅ
25
20
15
10
5
0
5
4
3
2
1
0

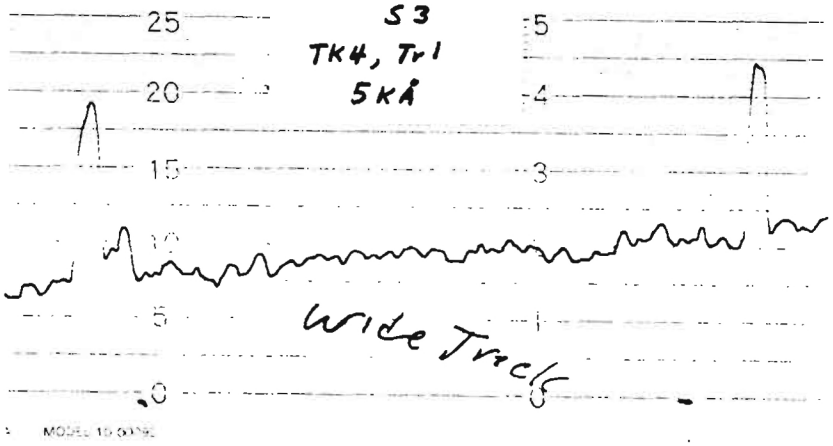
S 3
TK 4, Tr 1
5KÅ
25
20
15
10
5
0
5
4
3
2
1
0
Wide Track

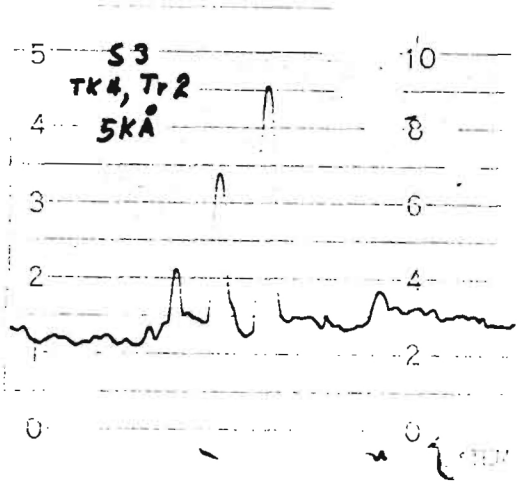
S 3
TK 4, Tr 2
5KÅ
5
4
3
2
1
0
10
8
6
4
2
0

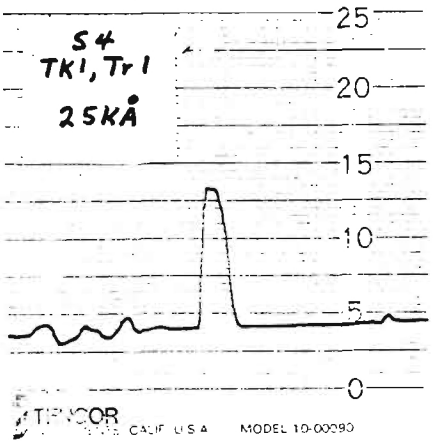
S4
TK1, Tr1
25KÅ
25
20
15
10
5
0
TENCOR
CALIF U.S.A
MODEL 10-00090

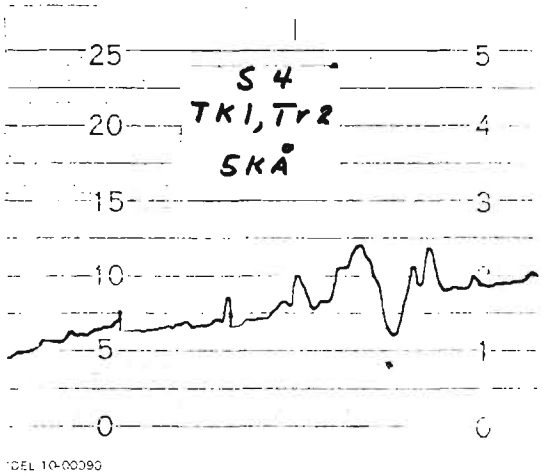
S4
TK1, Tr2
5KÅ
25
20
15
10
5
5
4
3
1
0
MODEL 10-00090

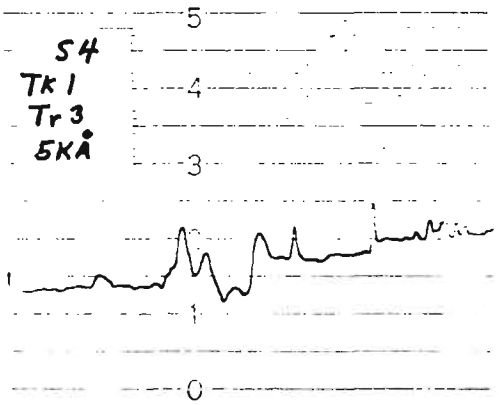
S4
Tk1
Tr3
5KÅ
5
4
3
1
0

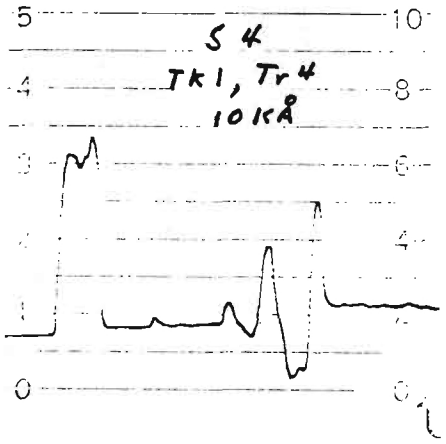
S4
TK1, Tr4
10KÅ
5
4
10
8
6
4
0

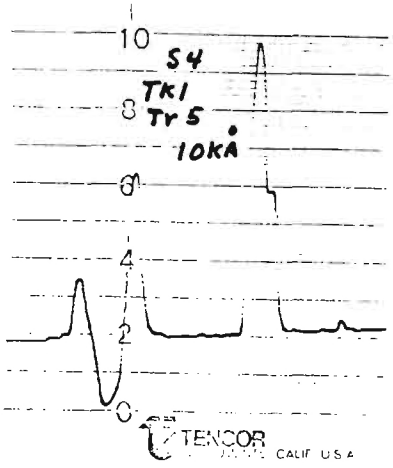
S4
TK1
Tr5
10KÅ
10
8
6
4
2
0
TENCOR
CALIF U.S.A

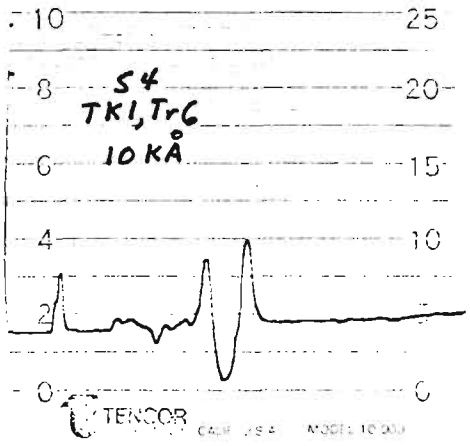
S4
TK1, TrC
10 KÅ
10
8
6
4
2
25
20
15
10
0
TENCOR

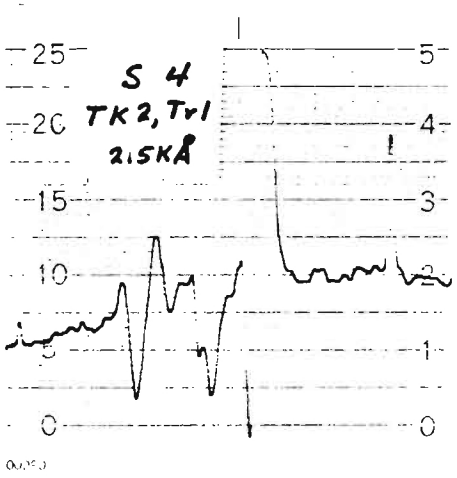

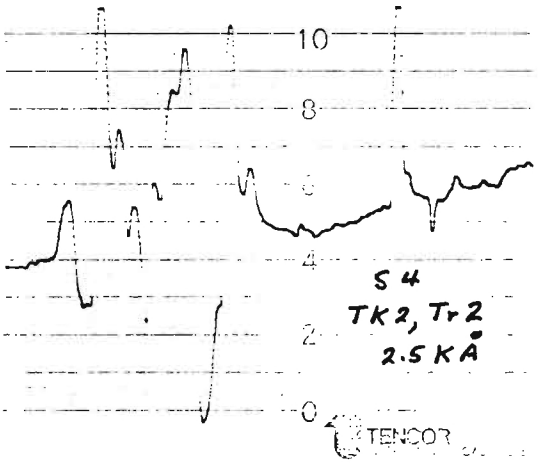

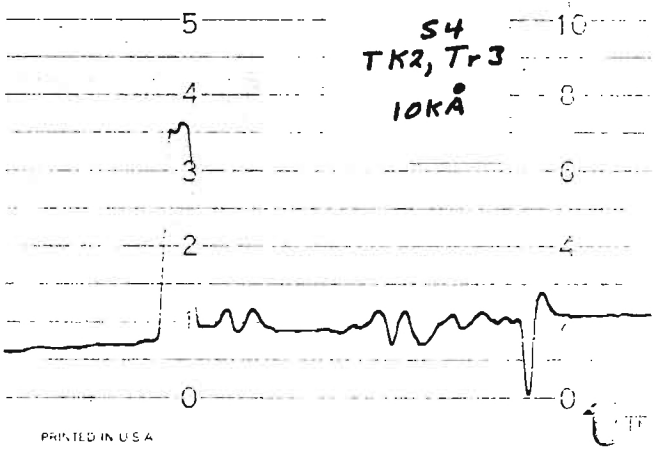

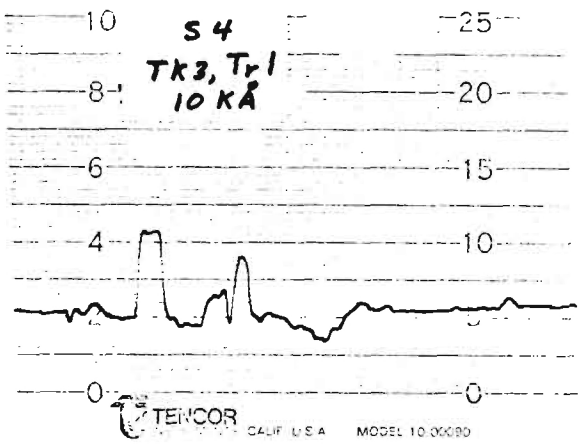
S 4
Tk 3, Tr 1
10 KÅ
10
8
6
4
0
25
20
15
10
0
TENCOR
CALIF U.S.A
MODEL 10 000/00

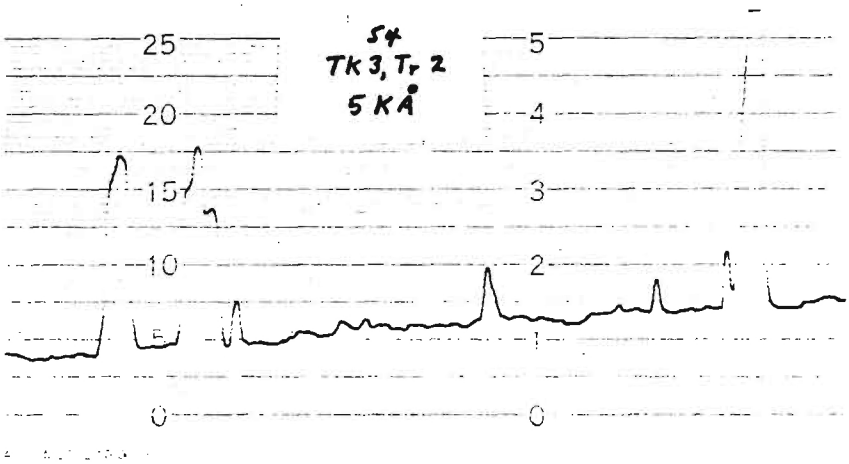
S 4
Tk 3, Tr 2
5 KÅ
25
20
15
10
0
5
4
3
2
1
0

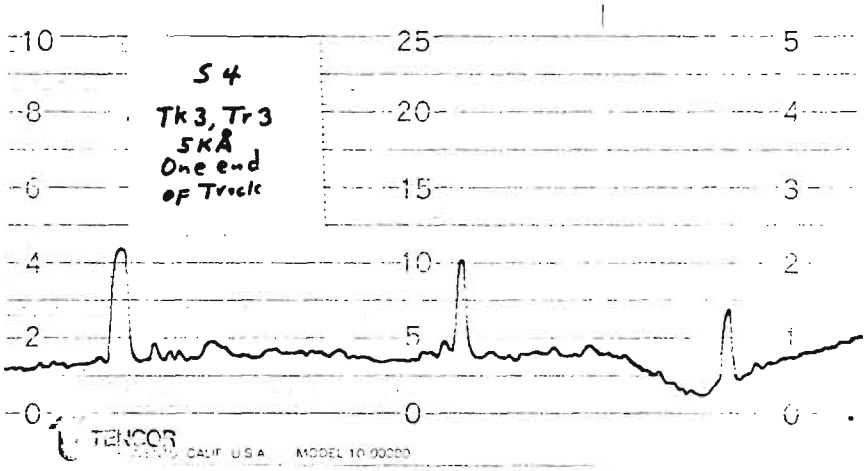
S 4
Tk 3, Tr 3
5 KÅ
One end
of Trace
10
8
6
4
2
0
25
20
15
10
5
0
5
4
3
2
1
0
TENCOR
CALIF U.S.A
MODEL 10 00000

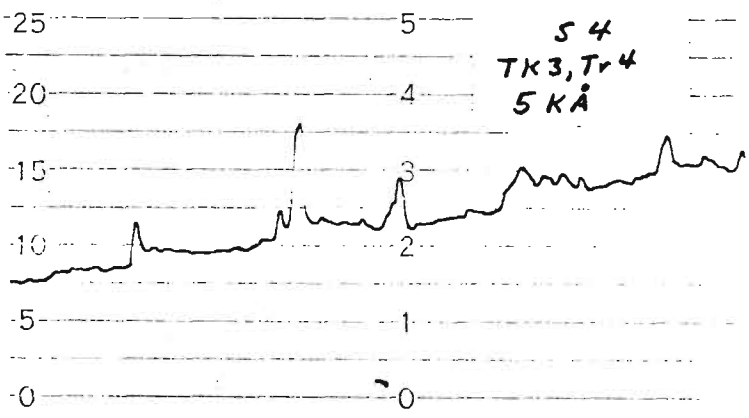
S 4
Tk 3, Tr 4
5 KÅ
25
20
15
10
5
0
5
4
3
2
1
0

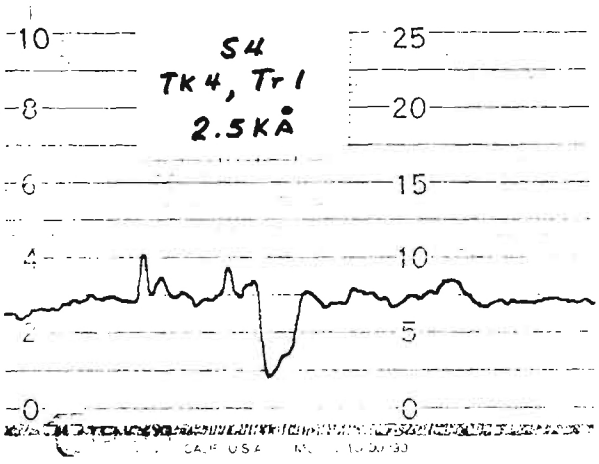
S4
TK4, Tr 1
2.5KÅ
10
8
6
4
2
0
25
20
15
10
5
0

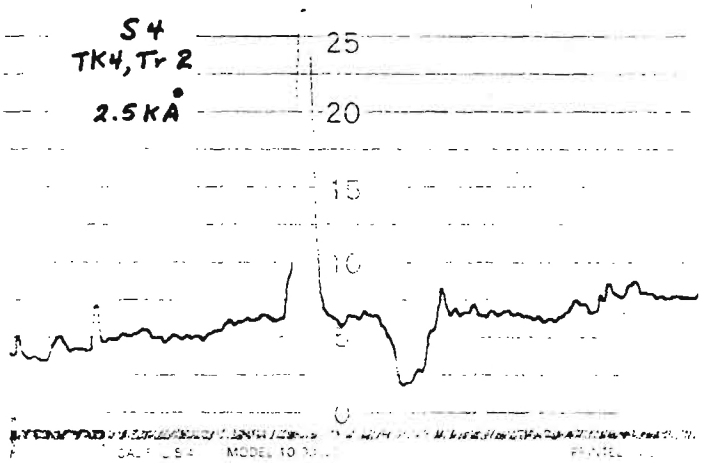
S4
TK4, Tr 2
2.5KÅ
25
20
15
10
5
0

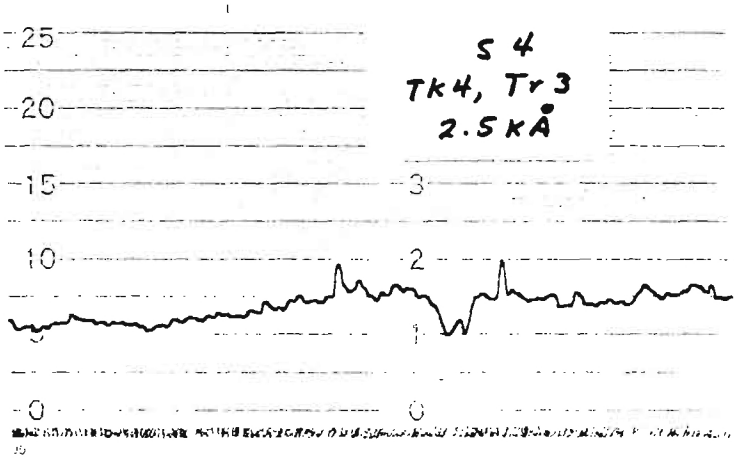
S 4
TK4, Tr 3
2.5KÅ
25
20
15
10
5
3
2
1
0

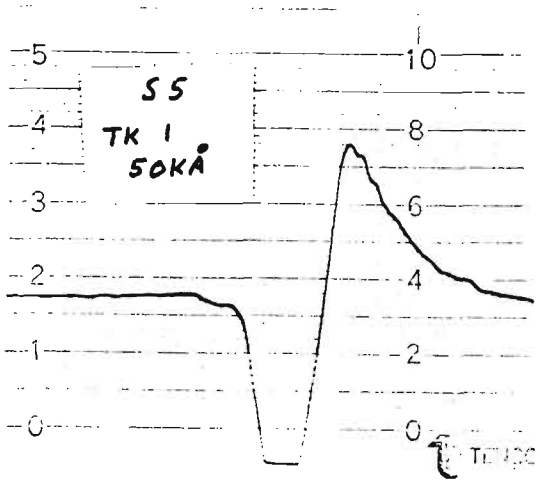
5
4
3
2
1
0
10
8
6
4
2
0
SS
TK 1
50KÅ

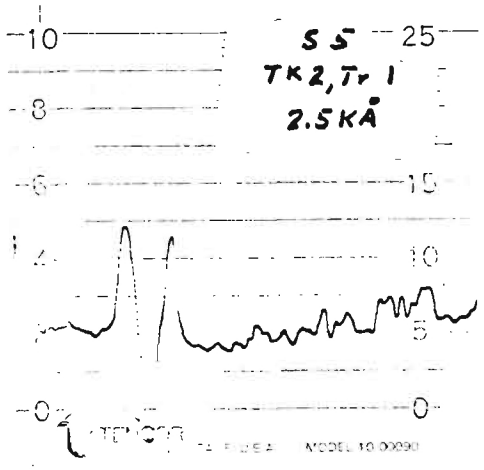
10
8
6
4
2
0
25
15
10
5
0
SS
TK2, Tr 1
2.5KÅ

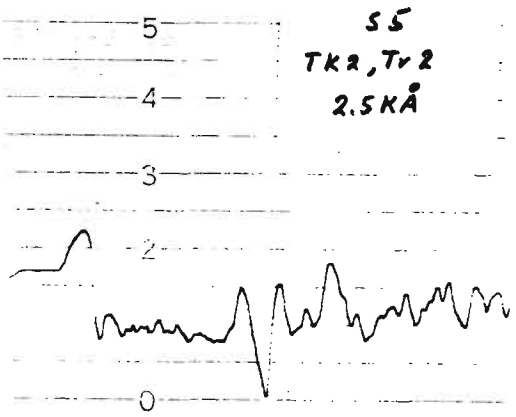
5
4
3
2
0
SS
TK2, Tr 2
2.5KÅ

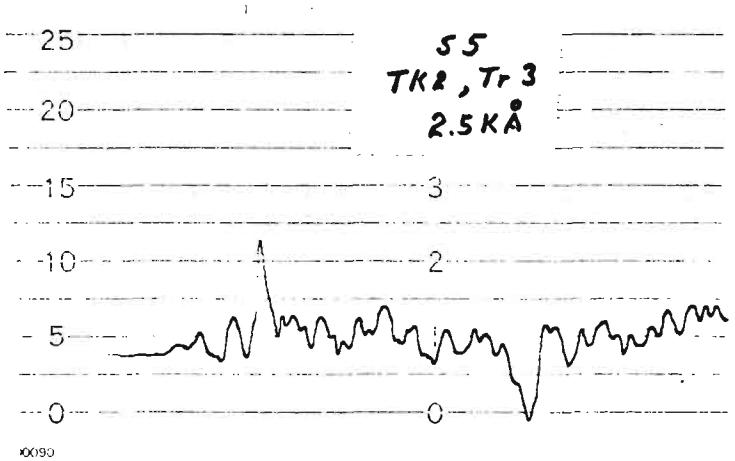
25
20
15
10
5
0
3
2
0
SS
TK2, Tr 3
2.5KÅ
90

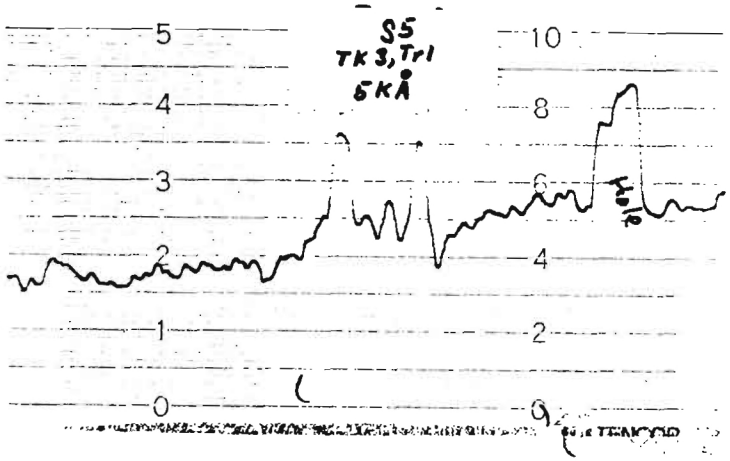
SS
TK3, Tr1
5KÅ

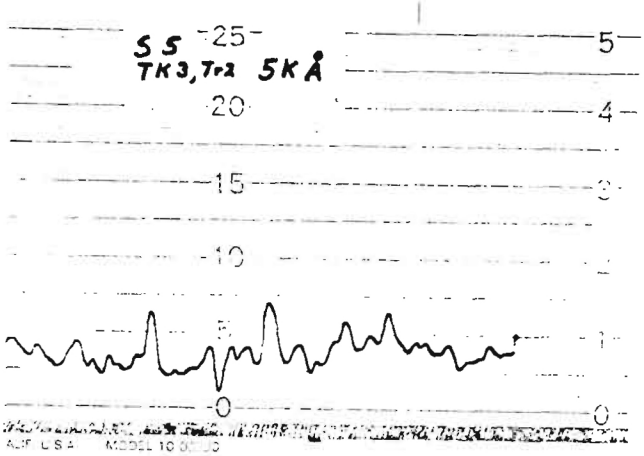
SS
TK3, Tr2 5KÅ

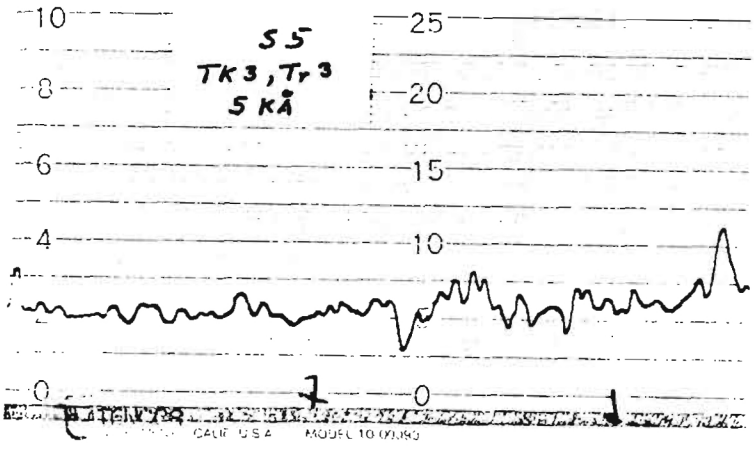
SS
TK3, Tr3
5 KÅ

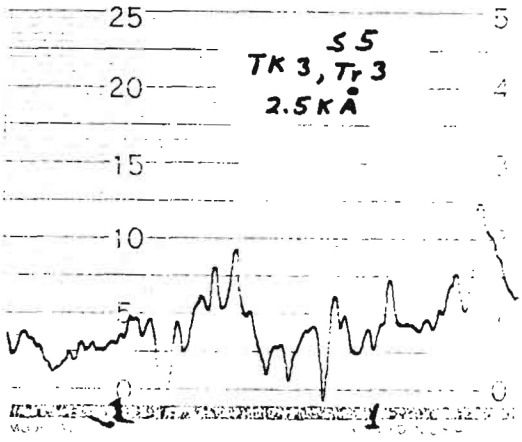
SS
TK3, Tr3
2.5KÅ

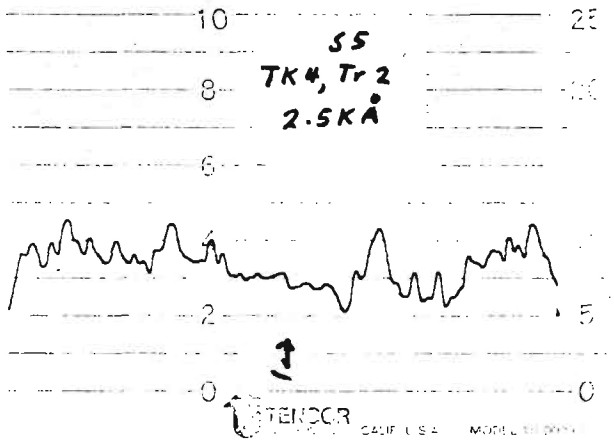
10
8
6
4
2
0
25
5
0
SS
TK4, Tr 2
2.5KA
1
TENCOR

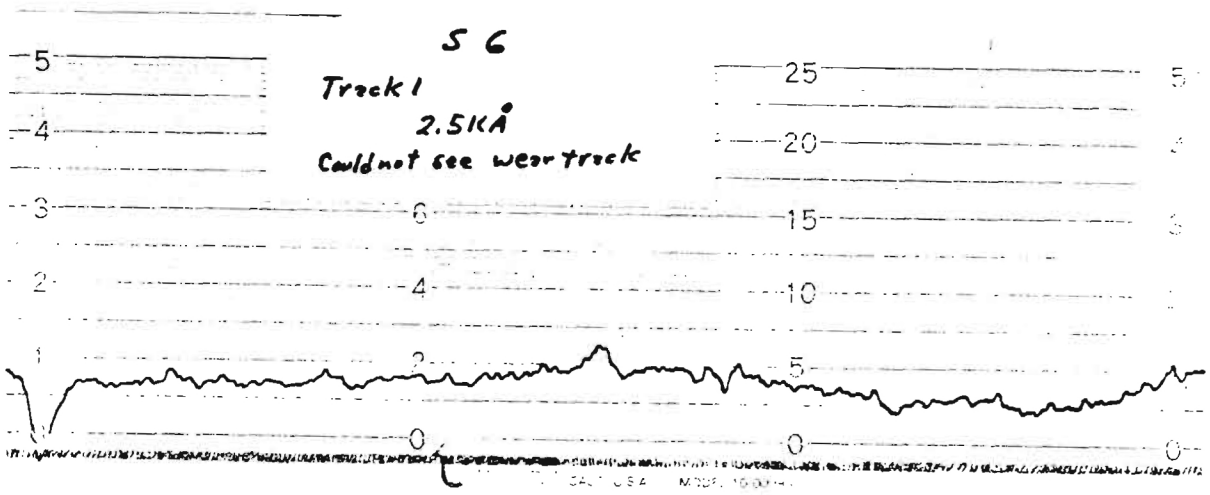
S C
Track 1
2.5KA
Could not see wear track
5
4
3
2
1
0
6
4
2
0
25
20
15
10
5
0

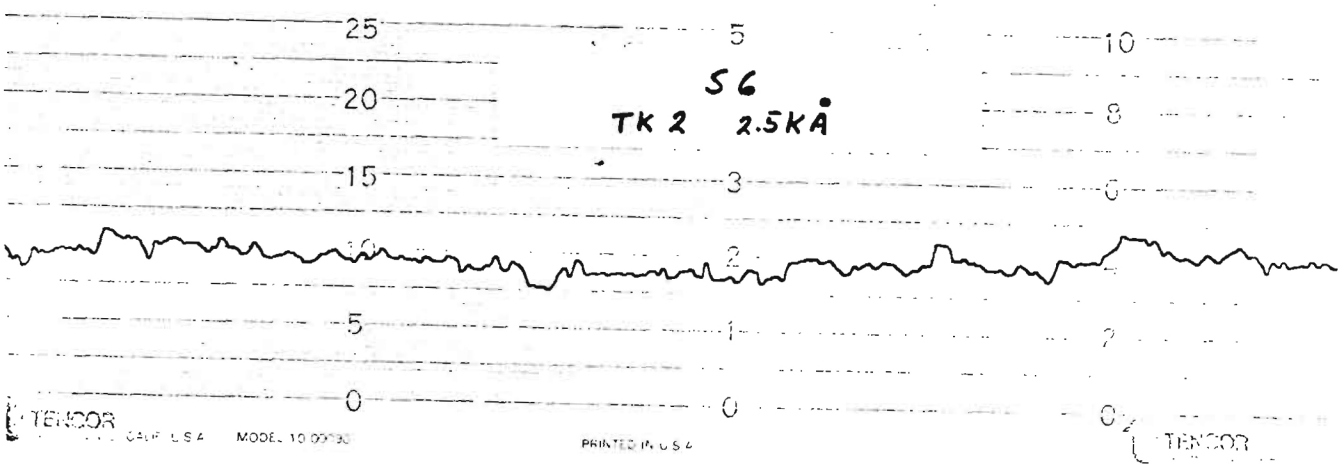
S C
TK 2 2.5KA
25
20
15
10
5
0
5
3
2
1
0
10
8
6
4
2
0
TENCOR
TENCOR

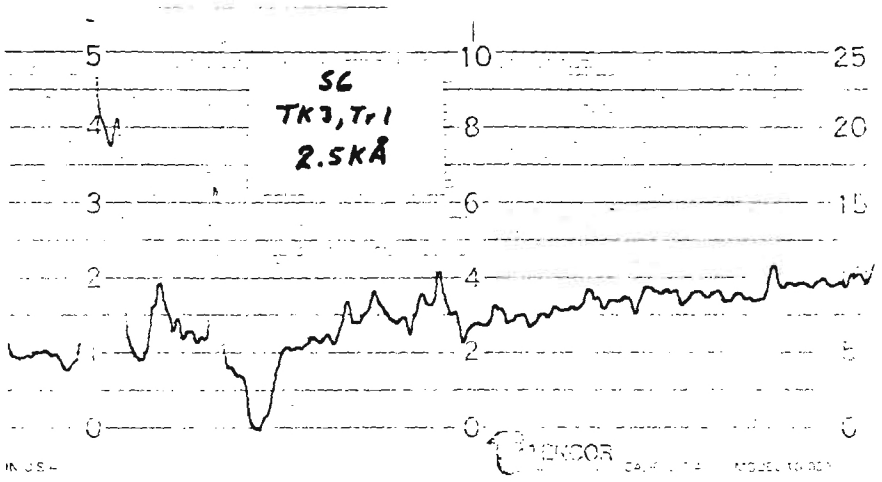
SC
TK3, Tr1
2.5KÅ
TENCOR

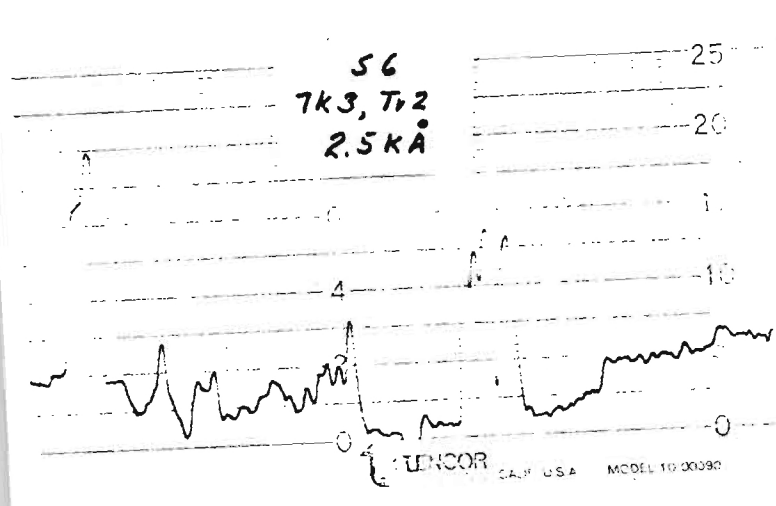
SC
TK3, Tr2
2.5KÅ
TENCOR
CALIF. U.S.A.
MODEL 10 00090

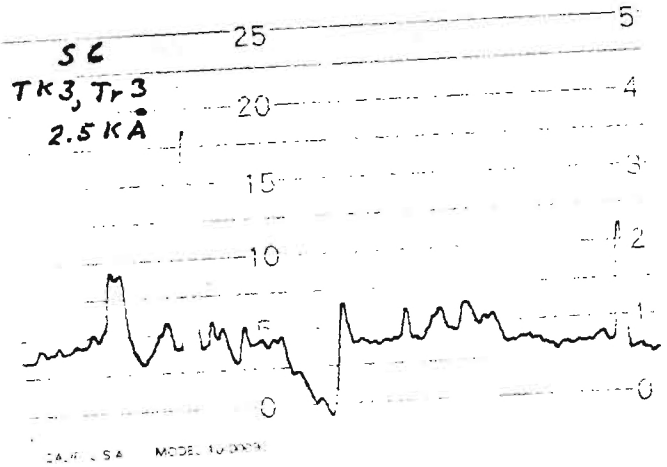
SC
TK3, Tr3
2.5KÅ

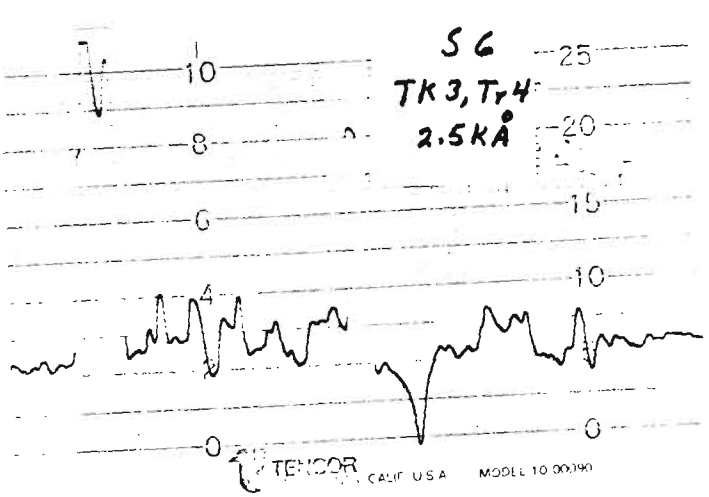
SC
TK3, Tr4
2.5KÅ
TENCOR
CALIF. U.S.A.
MODEL 10 00090

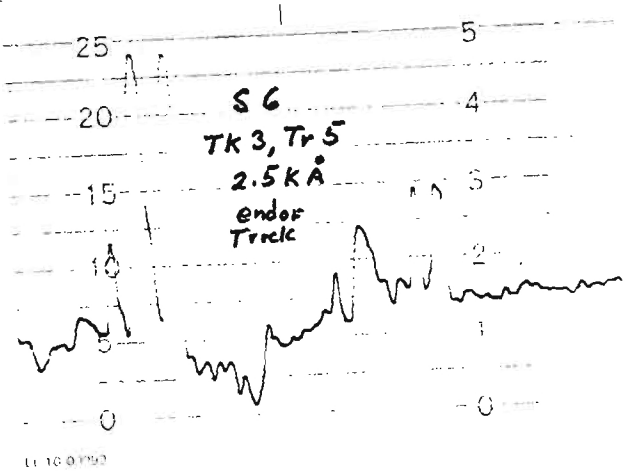
SC
TK3, Tr5
2.5KÅ
endor
Trace

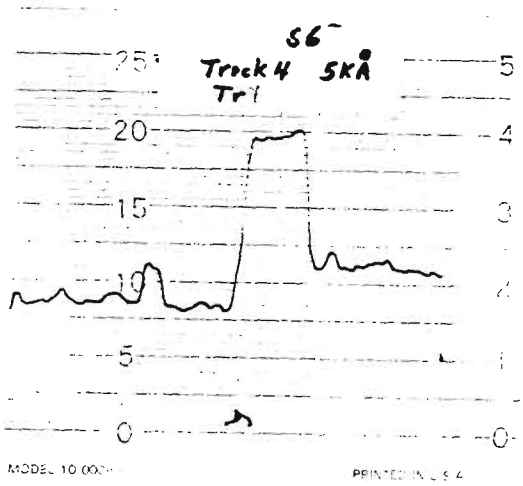
SG
Track 4 5KÅ
Tr 1
25
20
15
10
5
0
5
4
3
2
1
0

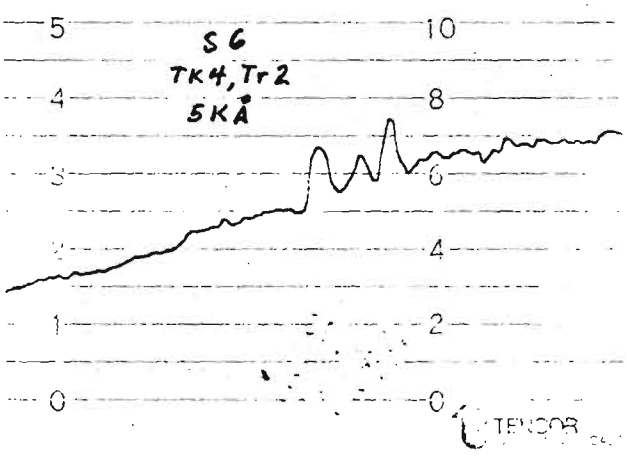
SG
TK4, Tr2
5KÅ
5
4
3
2
1
0
10
8
6
4
2
0
TENCOR